An implicit–gradient–enhanced incremental–secant mean-field homogenization scheme for elasto–plastic composites with damage

L. Wu[a,*], L. Noels[a], L. Adam[b], I. Doghri[b,c]

[a] *University of Liege, Department of Aeronautics and Mechanical Engineering – Computational & Multiscale Mechanics of Materials (CM3) Chemin des Chevreuils 1, B-4000 Liège, Belgium*
[b] *e-Xstream Engineering, Axis Park-Building H Rue Emile Francqui 9, B-1435 Mont–Saint–Guibert, Belgium*
[c] *Université Catholique de Louvain, Bâtiment Euler, 1348 Louvain-la-Neuve, Belgium*

Abstract

This paper presents an incremental–secant mean-field homogenization (MFH) procedure for composites made of elasto–plastic constituents exhibiting damage. During the damaging process of one phase, the proposed method can account for the resulting unloading of the other phase, ensuring an accurate prediction of the scheme. When strain softening of materials is involved, classical finite element formulations lose solution uniqueness and face the strain localization problem. To avoid this issue the model is formulated in a so–called implicit gradient–enhanced approach, with a view toward macro-scale simulations. The method is then used to predict the behavior of composites whose matrix phases exhibit strain softening, and is shown to be accurate compared to unit cell simulations and experimental results. Then the convergence of the method upon strain softening, with respect to the mesh size, is demonstrated on a notched composite ply. Finally, applications consisting in a stacking plate, successively without and with a hole, are given as illustrations of the possibility of the method to be used in a multiscale framework.

Keywords: Mean–Field Homogenization, Composites, Damage, Non-local, Incremental–Secant

*Corresponding author, Phone: +32 4 366 94 53, Fax: +32 4 366 95 05
Email address: L.Wu@ulg.ac.be, (L. Wu)

1. Introduction

Homogenization methods can predict the macro or meso–scopic response of heterogeneous materials from their micro–structure constituents properties, with an acceptable accuracy, while being much more computationally efficient than direct numerical simulations. Among those methods, the mean–field homogenization (MFH) approach is a (semi–)analytical framework for the modeling of multi–phase composites. MFH methods were first developed for linear elastic composite materials by extending the Eshelby (1957) single inclusion solution to multiple inclusions interacting in an average way in the composite material. Most common extensions of the Eshelby solution are the Mori–Tanaka scheme developed by Mori and Tanaka (1973); Benveniste (1987) and the self-consistent scheme pioneered by Kröner (1958); Hill (1965b). MFH schemes can also be developed in the non-linear range to account for non–linear behaviors of the composite's constituents. Most of these extensions revolve around the definition of a so-called linear comparison composite (LCC) (Talbot and Willis, 1985, 1987; Ponte Castañeda, 1991, 1992; Talbot and Willis, 1992; Molinari et al., 2004), which is a virtual linear composite whose constituents behaviors match the linearized behaviors of the real constituents for given strain states. Besides MFH methods, non-linear effects can be considered by other homogenization methods, such as the method of cells proposed by Lissenden and Arnold (1997); Aboudi et al. (2003), the unit cell finite element (FE)–based computations as performed by Wieckowski (2000); Segurado et al. (2002); Ji and Wang (2003); Carrere et al. (2004), or again such as the multiscale FE2 method pioneered by Kouznetsova et al. (2002, 2004) as a non-exhaustive list. Kanouté et al. (2009); Geers et al. (2010) have presented overviews of the different homogenization methods.

Although multiscale homogenization methods have achieved an acceptable level of accuracy to capture the non-linear behavior of composites (Pierard et al., 2007), accounting for material degradation, through damage or fracture models, remains highly challenging as discussed by Geers et al. (2010); LLorca et al. (2011). Besides the complexity of formulating such a multiscale method, the governing partial differential equations lose ellipticity at strain-softening onset, losing the uniqueness of the FE solution.

Many enhanced physical or phenomenological models, which introduce higher–order terms in the continuum, were proposed to avoid the strain localization issue, such as in the Cosserat model reformulated by De Borst

(1991), the non–local model pioneered by Bažant et al. (1984) or the gradient model, as exploited by Zbib and Aifantis (1989). Because of the presence of higher order terms, the interactions between neighboring material points are reflected in these models through an internal length, which is related to the micro-structure and the failure mechanisms of the material. An overview of these methods was presented by De Borst et al. (1993). One possible difficulty, with the existence of higher–order terms in the continuum, lies in the requirement of developing finite elements with higher-order derivatives continuity to evaluate explicitly internal variable derivatives, such as the strain gradient. To alleviate this complexity, the non-local kernel has been reformulated by Peerlings et al. (1996); Geers (1997); Peerlings et al. (1998) in an implicit way such that a new non-local variable, representative of an internal variable and its derivatives, results from the resolution of a new boundary value problem. Besides the advantage of using C^0 elements, although the elements have now one additional degree–of–freedom per node, this approach also possesses the feature of being fully non-local as it is constructed on the basis of a weighted averaging integral under the form of a new partial differential equation, contrarily to non-local models constructed on the incorporation of higher–order terms as for the models of Aifantis (1992); Svedberg and Runesson (1997).

Although such high–order and non–local formulations have been widely used in direct numerical simulations, their applications in multiscale computations are not commonly developed. When considering semi–analytical homogenization processes, Liu and Hu (2005) have applied the Cosserat model in the Mori–Tanaka procedure to study the particle size dependency of composite materials, Dascalu (2009) has connected the locally periodic micro–crack with the macroscopic damage through an asymptotic homogenization, and Knockaert and Doghri (1999) have introduced, in a 1D framework, the gradients of the internal variables, which are obtained from a micro/macro homogenization procedure, at the macro–scale computation. When considering numerical computational homogenizations, Massart et al. (2005, 2007) have considered the non–local approach at the micro–scale in the framework of the computational homogenization for the problem of masonry, and Coenen et al. (2011a,b) have extended this method in a more general setting.

Recently, Wu et al. (2012) –the authors– have proposed a MFH analysis allowing softening at the micro-scale and at the macro–scale to be captured without causing localization. In order to avoid the strain/damage localization caused by the matrix material softening, the implicit non–local formula-

tion (Peerlings et al., 2001; Engelen and Baaijens, 2003) was adopted during the homogenization process. In this formulation, the non–local accumulated plastic strain of the matrix is defined and depends on the local accumulated plastic strain and on its derivatives through the resolution of a new boundary value problem following the developments of Peerlings et al. (1996); Geers (1997); Peerlings et al. (1998).

The formulation presented by Wu et al. (2012) was based on the incremental–tangent MFH pioneered by Hill (1965a). This formulation defines the LCC from linearized relations between the stress and strain increments of the different constituents around their current strain states. Thus, the classical homogenization techniques for linear responses can still be used on the strain increments to predict the behaviors of elasto–plastic composites, as developed by Pettermann et al. (1999); Doghri and Ouaar (2003); Doghri and Tinel (2005); Pierard and Doghri (2006b). The MFH scheme developed by Wu et al. (2012), for composites whose matrix phase obeys an elasto–plastic law with non-local damage enhancement, was shown to have a reduced accuracy for high volume fractions of fibers when compared to the direct numerical simulations of a representative volume element (RVE), due to the recourse to an incremental–tangent formulation. Indeed, during the strain softening of the matrix, the fibers should see an elastic unloading due to the damaging process in the matrix, which cannot be modeled using this incremental–tangent approach. Therefore, it appears clear that the method should be reformulated within a different MFH framework.

Another existing MFH method is the affine method, which applies the mean–field homogenization on the total strain field as proposed by Molinari et al. (1987, 2004) for visco-plastic materials, and by Zaoui and Masson (2002); Masson et al. (2000) for elasto–plastic materials. Chaboche et al. (2005) showed that this method can lead to too stiff results when an anisotropic tangent operator is considered in the homogenization process. The accuracy of this method for visco-plastic composites has been improved by Pierard and Doghri (2006a); Mercier and Molinari (2009); Doghri et al. (2010). When considering damage, the affine method potentially suffers from the same over–estimation limitation as the incremental tangent method. The LCC can also be defined from a secant operator, which is joining the origin to the current strain/stress state, as initially proposed by Berveiller and Zaoui (1978) for elasto–plastic materials. However, this secant method is limited to monotonic and proportional loading paths.

The MFH methods previously described only consider first–statistical–

moment values of the strain and stress fields during the homogenization process. This can lead to poor predictions in the elasto–plastic case, as shown by Moulinec and Suquet (2003). This motivated to consider the second–statistical–moment (Ponte Castañeda, 1996) during the homogenization process. Such methods have been proposed for the secant formulations by Suquet (1995); Ponte Castañeda (2002a,b) and for the incremental–tangent formulation by Doghri et al. (2011). Suquet (1995) actually showed that the variational forms pioneered by Ponte Castañeda (1992) correspond to a second–order secant formulation, which was called modified secant. Finally, incremental variational formulations, which also correspond to a second–moment estimation, were recently proposed for visco-elastic composites by Lahellec and Suquet (2007a,b), for thermo–elastic composites by Lahellec et al. (2011), for elasto–(visco–)plastic composites by Brassart et al. (2011, 2012) and for elasto–visco–plastic composites with isotropic and kinematic hardening laws by Lahellec and Suquet (2013). However introducing damage models in combination with second–moment MFH methods is still an open area.

In order to remain accurate for materials exhibiting strain softening, it is mandatory to allow the fibers to be elastically unloaded when the stress field in the matrix decreases due to the degradation process. Recently, Wu et al. (Submitted) proposed a new first–moment incremental–secant MFH approach for elasto–plastic materials. In the formulation, at a given strain/stress state of the composite material, a virtual unloading step is applied on the composite level and the residual stresses are evaluated in both phases. Thus a secant approach is applied from this unloaded stage to define the LCC. This method was shown to be simple to implement and to predict results with an accuracy comparable to other MFH schemes for elasto–plastic materials, for short and long fiber composite materials, and also to be fit for monotonic and non–monotonic loadings.

It is intended in this paper to extend this incremental–secant MFH to composites whose matrix exhibits a damaging process. Because of the virtual elastic unloading step involved in the formulation the method remains highly accurate during the softening stage of the composite, even for high fiber volume fractions. This non–local multiscale method is also implemented in a finite element code to simulate problems at the laminate level.

The paper is organized as follows. Section 2 presents generalities on the MFH, as well as the main ideas of the incremental–secant MFH approach for elasto–plastic materials without damage. Section 3 presents the extension of

the incremental–secant MFH for materials exhibiting damage, after having recalled the mechanics of elasto–plastic materials exhibiting damage in a non-local setting. The prediction of the behavior of fiber–reinforced elasto–plastic matrix is demonstrated, in Section 4, to be more accurate than with the previously developed non–local incremental–tangent method, as the softening response is better captured. The model is also validated against experimental results for a metal matrix composite material. In Section 5, the convergence of the method with respect to the mesh size is illustrated on a notched sample. Finally the model is applied to study the response of laminates. First the material model is validated againt experiment by considering tensile tests including unloading on unidirectional carbon–fibers reinforced epoxy coupons. Then specimens made of the same laminate, but having a hole to force the localization, are considered. In this last example it can be seen that the damage–enhanced MFH captures the damage path oriented along the ply fiber directions in agreement with experimental results.

2. Incremental–secant MFH for elasto–plastic composites without damage

In this section concepts of the MFH for linear and non–linear composite materials are first presented before introducing the key ideas of the incremental–secant MFH.

2.1. Generalities on MFH

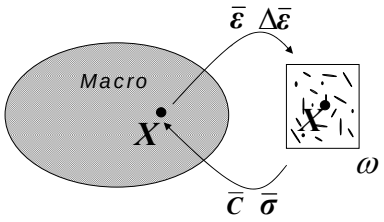

Figure 1: Multiscale method.

Figure 1 represents a classical multiscale approach: at each macro-point $\boldsymbol{X}$ the macro-strain $\bar{\boldsymbol{\varepsilon}}$ is known and the macro-stress $\bar{\boldsymbol{\sigma}}$ is sought through the resolution of a micro-scale boundary value problem (BVP). Toward this end, the macro-point is viewed at the micro-level as the center of a RVE of domain

$\boldsymbol{x} \in \omega$ and boundary $\partial\omega$. Then, the Hill-Mandell condition, expressing the equality between energies at both scales, transforms the relation between macro-strains $\bar{\boldsymbol{\varepsilon}}$ and stresses $\bar{\boldsymbol{\sigma}}$ into a relation between average strains $\langle\boldsymbol{\varepsilon}\rangle$ and stresses $\langle\boldsymbol{\sigma}\rangle$ over the RVE, with $\langle f(\boldsymbol{x})\rangle = \frac{1}{V_\omega}\int_\omega f(\boldsymbol{x})\mathrm{d}V$.

For two–phase composite materials of matrix subdomain ω_0 and of inclusions subdomain ω_I –subscripts 0 and I refer respectively to the matrix and to the inclusions, the macro–strains $\bar{\boldsymbol{\varepsilon}}$ and stresses $\bar{\boldsymbol{\sigma}}$ can be expressed as

$$\bar{\boldsymbol{\varepsilon}} = v_0\langle\boldsymbol{\varepsilon}\rangle_{\omega_0} + v_\mathrm{I}\langle\boldsymbol{\varepsilon}\rangle_{\omega_\mathrm{I}}\,, \quad \text{and} \tag{1}$$

$$\bar{\boldsymbol{\sigma}} = v_0\langle\boldsymbol{\sigma}\rangle_{\omega_0} + v_\mathrm{I}\langle\boldsymbol{\sigma}\rangle_{\omega_\mathrm{I}}\,, \tag{2}$$

with the phase volume ratios satisfying $v_0 + v_\mathrm{I} = 1$. For simplicity, in the following developments, the notations $\langle\bullet\rangle_{\omega_i}$ will be replaced by $\bullet_i$.

The relation between the average incremental strains in the two phases in the case of non–linear behaviors relies on the definition of a so–called linear comparison composite (LCC), which is characterized by the expressions of the virtual elastic operators $\bar{\boldsymbol{C}}_0^{\mathrm{LCC}}$ of the matrix phase and $\bar{\boldsymbol{C}}_\mathrm{I}^{\mathrm{LCC}}$ of the inclusions phase I, leading to

$$\Delta\boldsymbol{\varepsilon}_\mathrm{I} = \boldsymbol{B}^\epsilon(\mathrm{I}, \bar{\boldsymbol{C}}_0^{\mathrm{LCC}}, \bar{\boldsymbol{C}}_\mathrm{I}^{\mathrm{LCC}}) : \Delta\boldsymbol{\varepsilon}_0\,. \tag{3}$$

This equation describes the relation between the averages of the strain increments per phase through the strain concentration tensor $\boldsymbol{B}^\epsilon$. Considering the Mori and Tanaka (1973) (M-T) assumption, the strain concentration tensor reads

$$\boldsymbol{B}^\epsilon = \{\boldsymbol{I} + \boldsymbol{S} : [(\bar{\boldsymbol{C}}_0^{\mathrm{LCC}})^{-1} : \bar{\boldsymbol{C}}_\mathrm{I}^{\mathrm{LCC}} - \boldsymbol{I}]\}^{-1}\,, \tag{4}$$

where the Eshelby (1957) tensor $\boldsymbol{S}(\mathrm{I}, \bar{\boldsymbol{C}}_0^{\mathrm{LCC}})$ depends on the geometry of the inclusions phase and on the virtual elastic operator $\bar{\boldsymbol{C}}_0^{\mathrm{LCC}}$. The expressions of the tensors $\bar{\boldsymbol{C}}_0^{\mathrm{LCC}}$ and $\bar{\boldsymbol{C}}_\mathrm{I}^{\mathrm{LCC}}$ depend on the chosen MFH process, and will be particularized in the next subsection for the incremental–secant method.

2.2. Incremental–secant MFH for elasto–plastic composites without damage

The development of an incremental–secant MFH formulation was motivated by the overestimation of the macro–response obtained by the previously developed incremental–tangent MFH when the matrix exhibits damage. Thus Wu et al. (Submitted) proposed to consider an unloading step before applying the MFH process, which leads to an incremental–secant formulation with per–phase residual strains. Such a formulation has been developed for

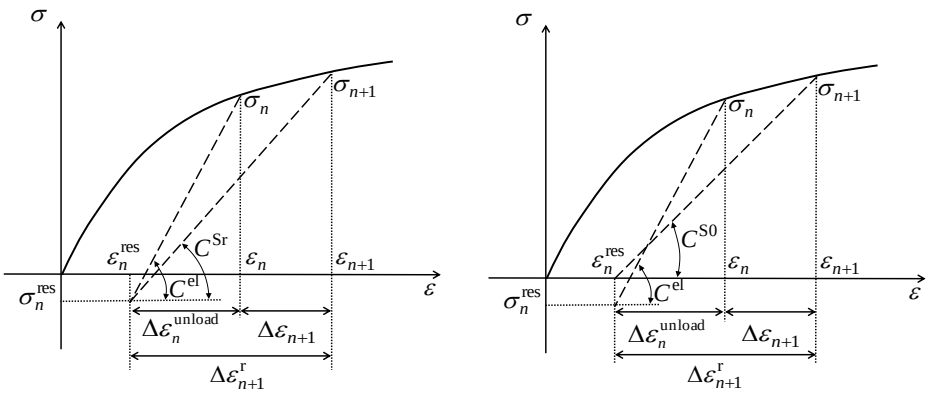

(a) Residual–secant (b) Zero–secant

Figure 2: Definition of the incremental–secant formulation, without considering damage. (a) Definition of the residual strain and stress and of the residual–secant operator. (b) Definition of the zero–secant operator.

elasto–plastic materials without considering damage, and will be extended to the damage case in this paper. In this section, the main ideas developed for elasto–plastic materials that do not exhibit damage are recalled.

Let us consider a time interval $[t_n,\ t_{n+1}]$. The total strain tensor at time t_n reads $\boldsymbol{\varepsilon}_n$ and the strain increment $\Delta\boldsymbol{\varepsilon}_{n+1}$ on the interval results from the finite element resolution yielding

$$\boldsymbol{\varepsilon}_{n+1} = \boldsymbol{\varepsilon}_n + \Delta\boldsymbol{\varepsilon}_{n+1}\,, \tag{5}$$

at time t_{n+1}, see Fig. 2(a). The key point of the incremental–secant method is to assume at time t_n a residual strain tensor $\boldsymbol{\varepsilon}_n^{\text{res}}$ that corresponds to an elastic unloading from the stress state $\boldsymbol{\sigma}_n$ to a stress state $\boldsymbol{\sigma}_n^{\text{res}}$. Note that this residual stress does not necessarily correspond to a zero–stress state. During the homogenization process, the residual stress for the homogenized composite material will be null while the different phases can have non–zero values.

2.2.1. Incremental–secant moduli for elasto–plastic phases

Considering an elasto–plastic phase of the composite material, the secant linearization of the elasto–plastic material is thus carried out in the time interval $[t_n,\ t_{n+1}]$ with the strain increment $\Delta\boldsymbol{\varepsilon}_{n+1}^{\text{r}}$, such that

$$\boldsymbol{\varepsilon}_{n+1} = \boldsymbol{\varepsilon}_n^{\text{res}} + \Delta\boldsymbol{\varepsilon}_{n+1}^{\text{r}}\,. \tag{6}$$

In this subsection, the indices related to the composite phase are omitted to simplify the notations. The stress tensor is now defined from the stress increment $\Delta\boldsymbol{\sigma}^{\mathrm{r}}_{n+1}$ following the incremental–secant approach depicted in Fig. 2(a):

$$\boldsymbol{\sigma}_{n+1} = \boldsymbol{\sigma}^{\mathrm{res}}_{n} + \Delta\boldsymbol{\sigma}^{\mathrm{r}}_{n+1}\,. \tag{7}$$

The stress increment is computed using $\boldsymbol{C}^{\mathrm{Sr}}$, the residual–incremental–secant operator of the elasto–plastic material, and following

$$\Delta\boldsymbol{\sigma}^{\mathrm{r}}_{n+1} = \boldsymbol{C}^{\mathrm{Sr}} : \Delta\boldsymbol{\varepsilon}^{\mathrm{r}}_{n+1}\,. \tag{8}$$

During the elastic response, this residual–incremental–secant operator corresponds to the elastic material tensor $\boldsymbol{C}^{\mathrm{el}}$. During the plastic flow, this operator is deduced by solving the following system of equations.

- The von Mises stress criterion reads

$$f\left(\boldsymbol{\sigma}_{n+1},\, p_{n+1}\right) = \boldsymbol{\sigma}^{\mathrm{eq}}_{n+1} - R(p_{n+1}) - \sigma_Y = 0\,, \tag{9}$$

  where f is the yield surface, $\boldsymbol{\sigma}^{\mathrm{eq}} = \sqrt{\frac{3}{2}\mathrm{dev}\left(\boldsymbol{\sigma}\right) : \mathrm{dev}\left(\boldsymbol{\sigma}\right)}$ is the equivalent von Mises stress, σ_Y is the initial yield stress, and $R(p) \geqslant 0$ is the isotropic hardening stress in terms of the accumulated plastic strain p, which is an internal variable characterizing the irreversible behavior.

- The Cauchy stress at time t_{n+1} is written as

$$\boldsymbol{\sigma}_{n+1} = \boldsymbol{\sigma}^{\mathrm{res}}_{n} + \boldsymbol{C}^{\mathrm{el}} : \Delta\boldsymbol{\varepsilon}^{\mathrm{r}}_{n+1} - \boldsymbol{C}^{\mathrm{el}} : \Delta\boldsymbol{\varepsilon}^{\mathrm{p}}\,,\ \text{with}\ \Delta\boldsymbol{\varepsilon}^{\mathrm{p}} = \Delta p \boldsymbol{N}_{n+1}\,, \tag{10}$$

  where $\boldsymbol{N}$ is the plastic flow direction. Within the incremental–secant approach, this direction is set to

$$\boldsymbol{N}_{n+1} \;=\; \frac{3}{2}\frac{\left(\boldsymbol{\sigma}_{n+1} - \boldsymbol{\sigma}^{\mathrm{res}}_{n}\right)^{\mathrm{dev}}}{\left(\boldsymbol{\sigma}_{n+1} - \boldsymbol{\sigma}^{\mathrm{res}}_{n}\right)^{\mathrm{eq}}}\,, \tag{11}$$

  which satisfies $\boldsymbol{N} : \boldsymbol{N} = \frac{3}{2}$ and $\Delta p = \sqrt{\frac{2}{3}\Delta\boldsymbol{\varepsilon}^{\mathrm{p}} : \Delta\boldsymbol{\varepsilon}^{\mathrm{p}}}$. On the one hand, if $\left(\boldsymbol{\sigma}^{\mathrm{res}}_{n}\right)^{\mathrm{dev}} = \boldsymbol{0}$ this last equation corresponds to $\boldsymbol{N}_{n+1} = \left(\frac{\partial f(\boldsymbol{\sigma}, p)}{\partial \boldsymbol{\sigma}}\right)_{n+1}$ and we have the classical relation. On the other hand, if $\left(\boldsymbol{\sigma}^{\mathrm{res}}_{n}\right)^{\mathrm{dev}} \neq \boldsymbol{0}$, $\boldsymbol{N}_{n+1}$ is a first–order approximation in terms of $\Delta\boldsymbol{\varepsilon}$ of the normal to the yield surface in the stress space. It has been shown in Wu et al. (Submitted)

that $\boldsymbol{N}_{n+1} = \boldsymbol{N}^{\mathrm{tr}}_{n+1}$, where the trial state "tr" corresponds to an elastic increment ($\Delta\boldsymbol{\varepsilon}^{\mathrm{p,\,tr}} = \boldsymbol{0}$). The elasto–plastic scheme consists of solving the equations (10) and $f\left(\boldsymbol{\sigma}_{n+1},\, p_{n+1}\right) = 0$, with $p_{n+1} = p_n + \Delta p$, in terms of Δp and $\boldsymbol{\sigma}^{\mathrm{eq}}_{n+1}$.

- It has been demonstrated by Wu et al. (Submitted) that the residual–incremental–secant operator of the linear comparison material, which can be computed from $\boldsymbol{\sigma}_{n+1}$, is isotropic for J2–plasticity, and that it reads

$$\boldsymbol{C}^{\mathrm{Sr}} = 3\kappa^{\mathrm{r}}\boldsymbol{I}^{\mathrm{vol}} + 2\mu^{\mathrm{r}}_s\boldsymbol{I}^{\mathrm{dev}}\,. \tag{12}$$

  The bulk modulus κ^{r} of the virtual elastic material is directly obtained as κ^{el} and the shear modulus μ^{r}_s of the virtual elastic material can be obtained by decomposing the increments of the stress and strain tensors into their hydrostatic and deviatoric parts, as detailed in Appendix B.1.

- The derivative of the operator (12) required during the upcoming MFH process is obtained following Appendix B.1.

- The incremental–secant–operator (12) can be used to define the LCC during the MFH process. One alternative proposed by Wu et al. (Submitted) follows the suggestion in Fig. 2(b). In that case the residual stress $\boldsymbol{\sigma}^{\mathrm{res}}_n$ is omitted in the described approach and the plastic flow direction (11) is rigorously normal to the yield surface. For this latter approach, the zero–incremental–secant operator of the linear comparison material reads

$$\boldsymbol{C}^{\mathrm{S0}} = 3\kappa^{0}\boldsymbol{I}^{\mathrm{vol}} + 2\mu^{0}_s\boldsymbol{I}^{\mathrm{dev}}\,, \tag{13}$$

  where κ^0 and μ^0_s are the elastic bulk and shear moduli of the virtual elastic material, respectively, obtained as detailed in Appendix B.1.

2.2.2. Incremental–secant MFH scheme

The stress tensor in the different composite material phases can be computed from a secant approach, following

$$\boldsymbol{\sigma}_{n+1} = \begin{cases} \boldsymbol{\sigma}^{\mathrm{res}}_n + \boldsymbol{C}^{\mathrm{Sr}} : \Delta\boldsymbol{\varepsilon}^{\mathrm{r}}_{n+1} & \text{for the residual–incremental–secant method;} \\ \boldsymbol{C}^{\mathrm{S0}} : \Delta\boldsymbol{\varepsilon}^{\mathrm{r}}_{n+1} & \text{for the zero–incremental–secant method.} \end{cases} \tag{14}$$

The secant operators can then be used in the MFH approach to define the LCC operators. Using these definitions of the LCCs, the MFH stated by Eqs. (1), (2) and (3) can thus be applied, and the system of equations is rewritten as

$$\Delta\bar{\boldsymbol{\varepsilon}}^{\mathrm{r}}_{n+1} = v_0\Delta\boldsymbol{\varepsilon}^{\mathrm{r}}_{0n+1} + v_{\mathrm{I}}\Delta\boldsymbol{\varepsilon}^{\mathrm{r}}_{\mathrm{I}n+1}\,, \tag{15}$$

$$\bar{\boldsymbol{\sigma}}_{n+1} = v_0\boldsymbol{\sigma}_{0n+1} + v_{\mathrm{I}}\boldsymbol{\sigma}_{\mathrm{I}n+1}\,, \tag{16}$$

with the stress tensor deriving from Eq. (14), and the relation between the strain increments reading

$$\Delta\boldsymbol{\varepsilon}^{\mathrm{r}}_{\mathrm{I}n+1} = \boldsymbol{B}^{\epsilon}(\boldsymbol{I}, \bar{\boldsymbol{C}}^{\mathrm{S}}_0, \bar{\boldsymbol{C}}^{\mathrm{S}}_{\mathrm{I}}) : \Delta\boldsymbol{\varepsilon}^{\mathrm{r}}_{0n+1}\,, \tag{17}$$

where $\bar{\boldsymbol{C}}^{\mathrm{S}}$ substitutes to either $\bar{\boldsymbol{C}}^{\mathrm{Sr}}$ or to $\bar{\boldsymbol{C}}^{\mathrm{S0}}$, the per–phase constant secant–operators resulting from the MFH process. The choice of the residual– or zero–incremental–secant operators will be discussed in the development of the MFH with damage. To complete these equations, the unloaded state is defined using $\bar{\boldsymbol{\sigma}}^{\mathrm{res}}_n = v_0\boldsymbol{\sigma}^{\mathrm{res}}_{0\ n} + v_{\mathrm{I}}\boldsymbol{\sigma}^{\mathrm{res}}_{\mathrm{I}\ n} = 0$.

The detailed MFH process is described in Wu et al. (Submitted).

3. Incremental–secant MFH for elasto–plastic composites with damage

In this section the incremental–secant MFH method summarized in Section 2.2 is extended to the non–local damage formulation. First the equations of elasto–plastic materials combined with a Lemaitre and Chaboche (1991) damage model are given in a non–local setting. Then the secant approach for one–phase materials is presented before eventually developing the incremental–secant MFH. The improvement of the prediction accuracy compared to the incremental–tangent MFH scheme will be illustrated for problems involving matrix softening in the next section.

3.1. Elasto–plastic materials with non–local enhanced damage models

The non–local implicit approach can be applied to damage models in order to avoid the loss of ellipticity at the macro-scale. Note that formulating the MFH in a local form can be done by considering the elasto–plastic model with damage also in a local form. Only the non–local case is considered herein, as the local form can be derived easily from the presented equations.

The damage is introduced with the usual assumption that the strain tensors observed in the actual body and in its undamaged representation are equivalent (Lemaitre, 1985), and the usual definition of the effective stress reads

$$\hat{\boldsymbol{\sigma}} = \frac{\boldsymbol{\sigma}}{(1-D)}\,, \tag{18}$$

where $\boldsymbol{\sigma}$ is the apparent Cauchy stress and where $0 \leq D < 1$ is the damage variable.

Assuming an elasto–plastic material, which obeys J2–elasto–plasticity, the von Mises stress criterion (9) is now written $f\left(\hat{\boldsymbol{\sigma}}, r\right) \leqslant 0$, where r is an internal variable related to the accumulated plastic strain p and to the plastic multiplier $\dot{\lambda}$ following $\dot{r} = \dot{\lambda} = (1-D)\dot{p}$, see (Doghri, 1995) for details. However in this paper we use the classical approximation that consists in writing the J2–plasticity in the effective stress space: $f\left(\hat{\boldsymbol{\sigma}}, p\right) \leqslant 0$.

During the plastic flow $f = 0$, $\Delta p > 0$ and the plastic strain tensor increment follows the plastic flow direction

$$\Delta\boldsymbol{\varepsilon}^{\mathrm{p}} = \Delta p \boldsymbol{N}\,, \tag{19}$$

where $\boldsymbol{N}$ is usually the normal to the yield surface in the effective stress space $\boldsymbol{N} = \frac{\partial f}{\partial \hat{\boldsymbol{\sigma}}} = \frac{3}{2}\frac{\mathrm{dev}(\hat{\boldsymbol{\sigma}})}{\hat{\boldsymbol{\sigma}}^{\mathrm{eq}}}$. Finally using the coupled damage concept leads to the stress expression at time t_{n+1}:

$$\boldsymbol{\sigma}_{n+1} = (1-D_{n+1})\boldsymbol{C}^{\mathrm{el}} : \left(\boldsymbol{\varepsilon}_{n+1} - \boldsymbol{\varepsilon}^{\mathrm{p}}_{n+1}\right) = (1-D_{n+1})\boldsymbol{C}^{\mathrm{el}} : \boldsymbol{\varepsilon}^{\mathrm{el}}_{n+1}\,. \tag{20}$$

What remains to be defined is the evolution of the damage. Following the technique proposed by Geers et al. (1998) to develop non–local damage laws, in this paper the non–local accumulated plastic strain $\tilde{p}$ is applied to calculate the damage evolution in the Lemaitre and Chaboche (1991) incremental model[1]:

$$\Delta D = \begin{cases} 0, & \text{if } \tilde{p} \leqslant p_C\ ; \\ (\frac{Y_{n+\alpha}}{S_0})^s \Delta\tilde{p}, & \text{if } \tilde{p} > p_C\,. \end{cases} \tag{21}$$

[1]In order to simplify the developments of the method, a scalar damage model is assumed. Although to remain more general, a damage variable should be represented by a tensor due to the existence of several mechanisms of damage, this is not necessary for damage induced by meso- or micro-plasticity as pointed out by Lemaitre and Desmorat (2005), which justifies the use of a simple model.

In this expression, p_C is a plastic threshold for the damage evolution, S_0 and s are the material parameters, Y is the strain energy release rate computed as

$$Y = \frac{1}{2}\boldsymbol{\varepsilon}^{\mathrm{el}} : \boldsymbol{C}^{\mathrm{el}} : \boldsymbol{\varepsilon}^{\mathrm{el}}\,, \tag{22}$$

and α is an interpolation parameter ranging from 0 to 1.

In this gradient enhanced damage model, the non–local accumulated plastic strain $\tilde{p}$ is computed from the implicit formulation

$$\tilde{p} - \nabla \cdot (\boldsymbol{c}_{\mathrm{g}} \cdot \nabla \tilde{p}) = p\,, \tag{23}$$

where $\boldsymbol{c}_{\mathrm{g}}$ is the characteristic lengths tensor as defined by Wu et al. (2013). For isotropic materials this tensor reads $\boldsymbol{c}_{\mathrm{g}} = \mathrm{diag}\,(c)$, with $c = l^2$ the square of the characteristic size. For composite materials, the anisotropy can be accounted for in this definition. As an example, for the matrix phase of a unidirectional (UD) continuous fiber-reinforced composite material, $c^i = (l^i)^2$ is different in the directions parallel and transverse to the inclusions. The tensor is thus computed from the rotation tensor $\boldsymbol{R}$ describing the inclusions orientation

$$\boldsymbol{c}_{\mathrm{g}} = \boldsymbol{R}^T \cdot \mathrm{diag}\left(c^i\right) \cdot \boldsymbol{R}\,. \tag{24}$$

Relation (23) is completed by the natural boundary condition

$$(\boldsymbol{c}_{\mathrm{g}} \cdot \nabla \tilde{p}) \cdot \boldsymbol{n} = 0\,. \tag{25}$$

The linearizations of the model with respect to $\boldsymbol{\varepsilon}$ and $\tilde{p}$ are provided in Appendix C.

3.2. Incremental–secant moduli with damage

The secant formulation described in Section 2.2 is extended herein to the non–local damage enhanced elasto–plastic case. We are still considering a time interval $[t_n,\ t_{n+1}]$, with the total strain tensor $\boldsymbol{\varepsilon}_n$ at time t_n and the strain increment $\Delta\boldsymbol{\varepsilon}_{n+1}$ resulting from the FE resolution and satisfying (5).

At time t_n, one can define an elastic unloading from the stress state $\boldsymbol{\sigma}_n$ –or from the effective stress state $\hat{\boldsymbol{\sigma}}_n$– that corresponds to a residual strain tensor $\boldsymbol{\varepsilon}_n^{\mathrm{res}}$, see Fig. 3. The main idea of the incremental–secant method, is to define a LCC, subjected to a strain increment $\Delta\boldsymbol{\varepsilon}_{n+1}^{\mathrm{r}}$, satisfying (6), and from

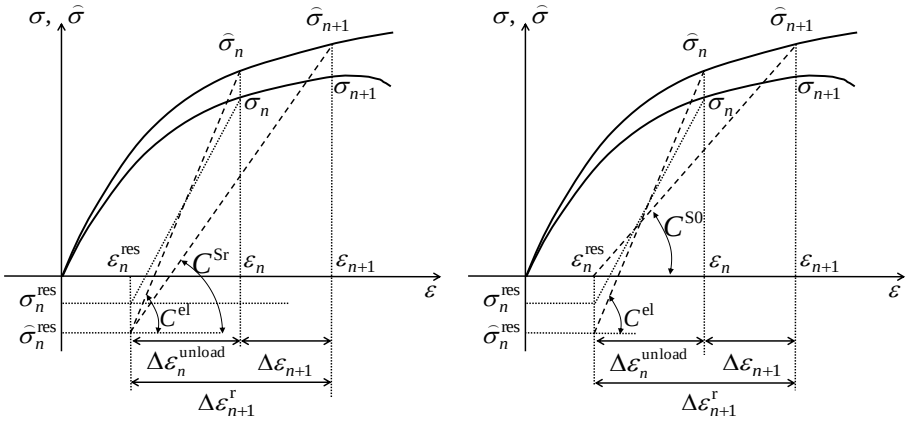

(a) Residual–secant (b) Zero–secant

Figure 3: Definition of the incremental–secant formulation when damage is considered. (a) Definition of the residual strain and stress and of the residual–secant operator. (b) Definition of the zero–secant operator.

which the stress tensor is computed. As for the case without damage, the two methods illustrated in Fig. 3 will be considered: the residual–incremental–secant method, which evaluates the effective stress tensor from the residual effective stress arising upon virtual unloading, and the zero–incremental–secant method, which evaluates the effective stress tensor from a zero–stress state.

3.2.1. Residual–incremental–secant approach

In the case of damage enhanced elasto–plastic materials, the secant formulation has to account for the effective and current stress tensors, with, $\hat{\boldsymbol{\sigma}}_n = \boldsymbol{\sigma}_n/(1-D_n)$ at time t_n. After the elastic unloading process the residual stress in each phase can be computed from, see Fig. 3(a)

$$\boldsymbol{\sigma}_n^{\mathrm{res}} = (1-D_n)\,\hat{\boldsymbol{\sigma}}_n^{\mathrm{res}} = (1-D_n)\,\hat{\boldsymbol{\sigma}}_n - (1-D_n)\,\boldsymbol{C}^{\mathrm{el}} : \Delta\boldsymbol{\varepsilon}_n^{\mathrm{unload}}\,. \tag{26}$$

During the time interval $[t_n,\, t_{n+1}]$ the stress reaches $\boldsymbol{\sigma}_{n+1}$, and the damage reaches D_{n+1}. Following the method pictured on Fig. 3(a), the effective stress tensor at time t_{n+1} can be rewritten as

$$\hat{\boldsymbol{\sigma}}_{n+1} = \hat{\boldsymbol{\sigma}}_n^{\mathrm{res}} + \Delta\hat{\boldsymbol{\sigma}}_{n+1}^{\mathrm{r}} \;\text{ and }\; \boldsymbol{\sigma}_{n+1} = (1-D_{n+1})\,\hat{\boldsymbol{\sigma}}_{n+1}\,, \tag{27}$$

where

$$\Delta\hat{\boldsymbol{\sigma}}_{n+1}^{\mathrm{r}} = \boldsymbol{C}^{\mathrm{Sr}} : \Delta\boldsymbol{\varepsilon}_{n+1}^{\mathrm{r}}\,. \tag{28}$$

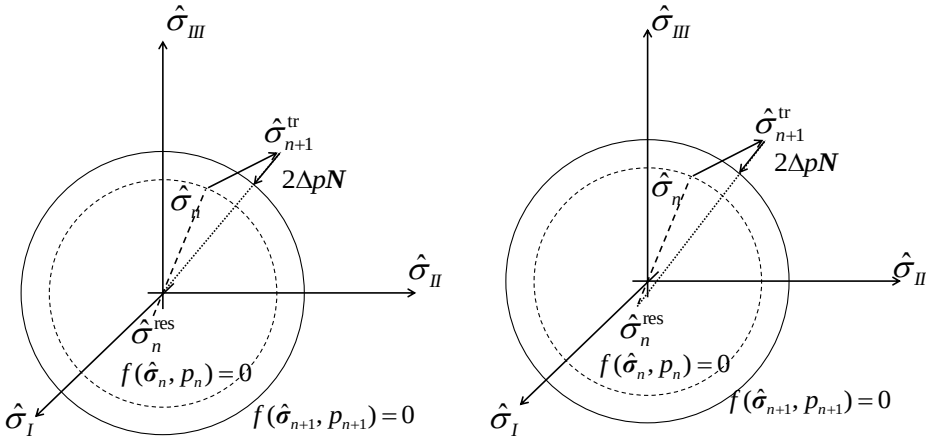

(a) Radial return mapping (b) Approximation

Figure 4: Plastic corrections in the effective stress space (a) Radial return mapping (b) Approximation (31).

In this last equation $\boldsymbol{C}^{\mathrm{Sr}}$ is the residual–incremental–secant operator of the undamaged linear comparison material.

During the elastic regime, the elastic tensor $\boldsymbol{C}^{\mathrm{el}}$ can be used as undamaged residual–incremental–secant operator. During elasto–plastic flow, the effective stress tensor $\hat{\boldsymbol{\sigma}}_{n+1}$ is computed from the unloaded state in the following way:

- Evaluate the trial effective stress tensor from an elastic response:

$$\hat{\boldsymbol{\sigma}}^{\mathrm{tr}}_{n+1} \;=\; \hat{\boldsymbol{\sigma}}_n + \boldsymbol{C}^{\mathrm{el}} : \Delta\boldsymbol{\varepsilon}_{n+1} = \hat{\boldsymbol{\sigma}}^{\mathrm{res}}_n + \boldsymbol{C}^{\mathrm{el}} : \Delta\boldsymbol{\varepsilon}^{\mathrm{r}}_{n+1}\,. \tag{29}$$

- If the trial effective stress tensor does not respect the von Mises criterion (9), *i.e.* $f\left(\hat{\boldsymbol{\sigma}}^{\mathrm{tr}}_{n+1},\, p_n\right) > 0$, then apply the plastic correction

$$\hat{\boldsymbol{\sigma}}_{n+1} = \hat{\boldsymbol{\sigma}}^{\mathrm{tr}}_{n+1} - \boldsymbol{C}^{\mathrm{el}} : \Delta\boldsymbol{\varepsilon}^{\mathrm{p}}\,,\ \text{with}\ \Delta\boldsymbol{\varepsilon}^{\mathrm{p}} = \Delta p\boldsymbol{N}_{n+1}\,. \tag{30}$$

  In this last equation, $\boldsymbol{N}$ is the plastic flow direction, which, extending the assumption discussed by Wu et al. (Submitted) from undamaged elasto–plasticity to damage coupling, reads

$$\boldsymbol{N}_{n+1} = \frac{3}{2}\frac{\left(\boldsymbol{C}^{\mathrm{Sr}} : \Delta\boldsymbol{\varepsilon}^{\mathrm{r}}_{n+1}\right)^{\mathrm{dev}}}{\left(\boldsymbol{C}^{\mathrm{Sr}} : \Delta\boldsymbol{\varepsilon}^{\mathrm{r}}_{n+1}\right)^{\mathrm{eq}}} = \frac{3}{2}\frac{\left(\hat{\boldsymbol{\sigma}}_{n+1} - \hat{\boldsymbol{\sigma}}^{\mathrm{res}}_n\right)^{\mathrm{dev}}}{\left(\hat{\boldsymbol{\sigma}}_{n+1} - \hat{\boldsymbol{\sigma}}^{\mathrm{res}}_n\right)^{\mathrm{eq}}}\,, \tag{31}$$

and which satisfies $\boldsymbol{N} : \boldsymbol{N} = \frac{3}{2}$. When $(\hat{\boldsymbol{\sigma}}_n^{\text{res}})^{\text{dev}} \neq 0$, $\boldsymbol{N}_{n+1}$ is a first order approximation of the normal to the yield surface in the effective stress space, see Fig. 4. Using Eqs. (29), (30) and (31), one can deduce

$$\boldsymbol{N} = \frac{3}{2} \frac{\left(\boldsymbol{C}^{\text{el}} : \Delta\boldsymbol{\varepsilon}_{n+1}^{\text{r}}\right)^{\text{dev}}}{\left(\boldsymbol{C}^{\text{el}} : \Delta\boldsymbol{\varepsilon}_{n+1}^{\text{r}}\right)^{\text{eq}}} \,, \tag{32}$$

as well as the system of equations to be solved as

$$(\hat{\boldsymbol{\sigma}}_{n+1} - \hat{\boldsymbol{\sigma}}_n^{\text{res}})^{\text{eq}} + 3\mu^{\text{el}}\Delta p = \left(\hat{\boldsymbol{\sigma}}_{n+1}^{\text{tr}} - \hat{\boldsymbol{\sigma}}_n^{\text{res}}\right)^{\text{eq}} \,, \text{ and} \tag{33}$$

$$f\left(\hat{\boldsymbol{\sigma}}_{n+1},\, p_{n+1}\right) = 0 \,, \tag{34}$$

with $p_{n+1} = p_n + \Delta p$.

- Knowing $\hat{\boldsymbol{\sigma}}_{n+1}$, and using Eqs. (28), (29), and (30) compute the residual–incremental–secant operator of the undamaged linear comparison material from

$$\Delta\hat{\boldsymbol{\sigma}}_{n+1}^{\text{r}} = \boldsymbol{C}^{\text{Sr}} : \Delta\boldsymbol{\varepsilon}_{n+1}^{\text{r}} = \boldsymbol{C}^{\text{el}} : \Delta\boldsymbol{\varepsilon}_{n+1}^{\text{r}} - 2\mu^{\text{el}}\Delta p\boldsymbol{N}_{n+1} \,, \tag{35}$$

which becomes after using Eq. (32)

$$\Delta\hat{\boldsymbol{\sigma}}_{n+1}^{\text{r}} = \left[\boldsymbol{C}^{\text{el}} - 3\mu^{\text{el}}\Delta p \frac{\boldsymbol{I}^{\text{dev}} : \boldsymbol{C}^{\text{el}}}{\left(\boldsymbol{C}^{\text{el}} : \Delta\boldsymbol{\varepsilon}_{n+1}^{\text{r}}\right)^{\text{eq}}}\right] : \Delta\boldsymbol{\varepsilon}_{n+1}^{\text{r}} = \boldsymbol{C}^{\text{Sr}} : \Delta\boldsymbol{\varepsilon}_{n+1}^{\text{r}} \,. \tag{36}$$

For J2–elasto–plastic materials, since $\boldsymbol{C}^{\text{el}}$ is isotropic, the residual–incremental–secant operator of the undamaged linear comparison material $\boldsymbol{C}^{\text{Sr}}$ is also isotropic. Moreover, as $\boldsymbol{C}^{\text{el}} = 3\kappa^{\text{el}}\boldsymbol{I}^{\text{vol}} + 2\mu^{\text{el}}\boldsymbol{I}^{\text{dev}}$, one can directly deduce

$$\boldsymbol{C}^{\text{Sr}} = 3\kappa^{\text{r}}\boldsymbol{I}^{\text{vol}} + 2\mu_s^{\text{r}}\boldsymbol{I}^{\text{dev}} \,, \tag{37}$$

with

$$\kappa^{\text{r}} = \kappa^{\text{el}} \,, \text{ and} \tag{38}$$

$$\mu_s^{\text{r}} = \mu^{\text{el}} - \frac{3{\mu^{\text{el}}}^2\Delta p}{\left(\boldsymbol{C}^{\text{el}} : \Delta\boldsymbol{\varepsilon}_{n+1}^{\text{r}}\right)^{\text{eq}}} = \mu^{\text{el}} - \frac{3{\mu^{\text{el}}}^2\Delta p}{(\hat{\boldsymbol{\sigma}}_{n+1} - \hat{\boldsymbol{\sigma}}_n^{\text{res}})^{\text{eq}}} \,. \tag{39}$$

- Practically the undamaged shear moduli of the virtual undamaged elastic comparison material can be obtained by decomposing the increments of the effective stress and strain tensors into their hydrostatic and deviatoric parts:

$$\Delta\hat{\boldsymbol{\sigma}}^{\mathrm{r}} = \Delta\hat{\sigma}^{m}\mathbf{1} + \Delta\hat{\boldsymbol{s}} \quad \text{and} \quad \Delta\boldsymbol{\varepsilon}^{\mathrm{r}} = \Delta\varepsilon^{m}\mathbf{1} + \Delta\boldsymbol{e}\,, \tag{40}$$

where $\Delta\hat{\sigma}^{m} = \frac{1}{3}\mathrm{tr}(\Delta\hat{\boldsymbol{\sigma}}^{\mathrm{r}})$, $\Delta\hat{\boldsymbol{s}} = \Delta\hat{\boldsymbol{\sigma}}^{\mathrm{r}} - \Delta\hat{\sigma}^{m}\mathbf{1}$, $\Delta\varepsilon^{m} = \frac{1}{3}\mathrm{tr}(\Delta\boldsymbol{\varepsilon}^{\mathrm{r}})$, and where $\Delta\boldsymbol{e} = \Delta\boldsymbol{\varepsilon}^{\mathrm{r}} - \Delta\varepsilon^{m}\mathbf{1}$, see Appendix A for the notations. Indeed, the increments of the von Mises equivalent stress and strain are respectively given by

$$\Delta\hat{\sigma}^{\mathrm{eq}} = \sqrt{\frac{3}{2}\Delta\hat{\boldsymbol{s}} : \Delta\hat{\boldsymbol{s}}} \quad \text{and} \quad \Delta\varepsilon^{\mathrm{eq}} = \sqrt{\frac{2}{3}\Delta\boldsymbol{e} : \Delta\boldsymbol{e}}\,, \tag{41}$$

and one has directly[2]

$$\mu_{s}^{\mathrm{r}} = \frac{\Delta\hat{\sigma}^{\mathrm{eq}}}{3\Delta\varepsilon^{\mathrm{eq}}}\,. \tag{42}$$

- Evaluate the damage D_{n+1} following the non–local Lemaitre–Chaboche model described in Section 3.1.

- Compute the final stress $\boldsymbol{\sigma}_{n+1}$ from $\hat{\boldsymbol{\sigma}}_{n+1}$. Using Eq. (27), one also deduces

$$\boldsymbol{\sigma}_{n+1} = (1 - D_{n+1})\,\hat{\boldsymbol{\sigma}}_{n}^{\mathrm{res}} + \underbrace{(1 - D_{n+1})\,\boldsymbol{C}^{\mathrm{Sr}}}_{\boldsymbol{C}^{\mathrm{SDr}}} : \Delta\boldsymbol{\varepsilon}_{n+1}^{\mathrm{r}}\,, \tag{43}$$

where the residual–incremental–secant operator of the damaged isotropic–linear comparison material reads

$$\boldsymbol{C}^{\mathrm{SDr}} = 3\kappa^{\mathrm{Dr}}\boldsymbol{I}^{\mathrm{vol}} + 2\mu_{s}^{\mathrm{Dr}}\boldsymbol{I}^{\mathrm{dev}}\,, \tag{44}$$

with the equivalent damaged bulk and shear elastic moduli κ^{Dr} and μ_{s}^{Dr} directly obtained from

$$\kappa^{\mathrm{Dr}} = (1 - D_{n+1})\,\kappa^{\mathrm{el}}\,, \text{ and} \tag{45}$$

$$\mu_{s}^{\mathrm{Dr}} = (1 - D_{n+1})\,\mu_{s}^{\mathrm{r}} = (1 - D_{n+1})\,\frac{\Delta\hat{\sigma}^{\mathrm{eq}}}{3\Delta\varepsilon^{\mathrm{eq}}}\,. \tag{46}$$

We need to clarify that the equivalent damaged bulk elastic modulus κ^{Dr} is not constant although the plastic flow is incompressible.

[2] If $\Delta\varepsilon^{\mathrm{eq}} = 0$, the indefiniteness is solved by considering $\mu_{s}^{\mathrm{r}} = \mu^{\mathrm{el}}$

- Evaluate the derivation of the operator (44) following Appendix B.2.

3.2.2. Zero–incremental–secant approach

As lengthy discussed by Wu et al. (Submitted), when defining the LCC, it can be advantageous to modify the residual–incremental–secant approach by neglecting the residual stress –but not the residual strain– in the matrix phase. The modification follows the suggestion illustrated in Fig. 2(b) and consists in neglecting $\hat{\boldsymbol{\sigma}}_n^{\mathrm{res}}$ in the formalism described here above, in which case

$$\begin{aligned} \boldsymbol{C}^{\mathrm{SD0}} &= (1-D_{n+1})\,\boldsymbol{C}^{\mathrm{S0}} \\ &= 3\underbrace{(1-D_{n+1})\,\kappa^0}_{\kappa^{\mathrm{D0}}}\boldsymbol{I}^{\mathrm{vol}} + 2\underbrace{(1-D_{n+1})\,\mu_s^0}_{\mu_s^{\mathrm{D0}}}\boldsymbol{I}^{\mathrm{dev}}\,, \end{aligned} \tag{47}$$

is the zero–incremental–secant operator of the damaged isotropic–linear comparison material expressed in terms of the equivalent damaged bulk and shear elastic moduli κ^{D0} and μ_s^{D0}. These values are readily obtained from

$$\kappa^{\mathrm{D0}} = \frac{\sigma^m}{3\Delta\varepsilon^m} = \frac{(1-D_{n+1})\hat{\sigma}^m}{3\Delta\varepsilon^m} = (1-D_{n+1})\,\kappa^{\mathrm{el}}\,, \text{ and} \tag{48}$$

$$\mu_s^{\mathrm{D0}} = \frac{\sigma^{\mathrm{eq}}}{3\Delta\varepsilon^{\mathrm{eq}}} = \frac{(1-D_{n+1})\hat{\sigma}^{\mathrm{eq}}}{3\Delta\varepsilon^{\mathrm{eq}}}\,. \tag{49}$$

The linearization of $\boldsymbol{C}^{\mathrm{SD0}}$ is given in Appendix B.2.

3.2.3. Incremental–secant approach summary

Two incremental–secant models have been considered, the first one accounting for the residual stress, see Fig. 3(a), and the other one formulated from a stress-free state, see Fig. 3(b), with

$$\hat{\boldsymbol{\sigma}}_{n+1} = \begin{cases} \hat{\boldsymbol{\sigma}}_n^{\mathrm{res}} + \boldsymbol{C}^{\mathrm{Sr}} : \Delta\boldsymbol{\varepsilon}_{n+1}^{\mathrm{r}} & \text{for the residual–incremental–secant;} \\ \boldsymbol{C}^{\mathrm{S0}} : \Delta\boldsymbol{\varepsilon}_{n+1}^{\mathrm{r}} & \text{for the zero–incremental–secant.} \end{cases} \tag{50}$$

In the current stress state, these two models read

$$\boldsymbol{\sigma}_{n+1} = \begin{cases} (1-D_{n+1})\,\hat{\boldsymbol{\sigma}}_n^{\mathrm{res}} + \boldsymbol{C}^{\mathrm{SDr}} : \Delta\boldsymbol{\varepsilon}_{n+1}^{\mathrm{r}} & \text{for the residual–incremental–secant;} \\ \boldsymbol{C}^{\mathrm{SD0}} : \Delta\boldsymbol{\varepsilon}_{n+1}^{\mathrm{r}} & \text{for the zero–incremental–secant.} \end{cases} \tag{51}$$

Note that in case of elastic response, the secant operator is the elastic tensor $\boldsymbol{C}^{\mathrm{el}}$.

As lengthy described by Wu et al. (Submitted) when no damage is considered, for composites with inclusions exhibiting an elasto–plastic behavior with a hardening coefficient lower than or of the same order as the one of the elasto–plastic matrix material, using the residual–incremental–secant operator for both phases leads to accurate predictions. However, for composites whose inclusions phase is much stiffer than the matrix material, such as elastic inclusions embedded in an elasto–plastic matrix or elasto–plastic inclusions with a high hardening compared to the one of the embedding elasto–plastic matrix, the zero–incremental–secant operator should be used in the matrix phase to avoid predicting over–stiff responses. With this restriction on the choice of the matrix operator, the method has been shown to predict the macro-stress with an accuracy level at least similar to those of the first–order incremental–tangent MFH method, or even advanced MFH schemes using per–phase statistical–second-moments of strain and stress fields. In the present case, we will keep the same combination of secant operators.

3.3. MFH scheme with non–local damage

In this section the incremental–secant MFH scheme presented in Section 2.2 is extended to the case of non–local elasto–plastic materials with damage, using the incremental–secant operators of the isotropic–linear comparison materials as defined in Section 3.2 to construct a LCC. Unless the expressions need to be particularized to the residual–incremental–secant or to the zero–incremental–secant forms, the isotropic linear comparison operator

$$\boldsymbol{C}^{\mathrm{SD}} = 3\kappa^{\mathrm{D}}\boldsymbol{I}^{\mathrm{vol}} + 2\mu_s^{\mathrm{D}}\boldsymbol{I}^{\mathrm{dev}}\,, \tag{52}$$

will substitute to either $\boldsymbol{C}^{\mathrm{SDr}}$ or $\boldsymbol{C}^{\mathrm{SD0}}$. Similarly, μ_s^{D} holds for either μ_s^{Dr} or for μ_s^{D0}, and κ^{D} holds for either κ^{Dr} or for κ^{D0}. In this paper, we consider a damage model only in the matrix phase.

Considering a time interval $[t_n,\ t_{n+1}]$, the system of governing equations of the homogenized material using the implicit gradient–enhanced elasto–plasticity is stated at time t_{n+1} by

$$\nabla\cdot\boldsymbol{\sigma}^{T}_{n+1} + \boldsymbol{f}_{n+1} = \boldsymbol{0} \qquad \text{for the homogenized material,} \tag{53}$$

$$\tilde{p}_{n+1} - \nabla\cdot(\boldsymbol{c}_{\mathrm{g}}\cdot\nabla\tilde{p}_{n+1}) = p_{n+1} \qquad \text{for the matrix material only,} \tag{54}$$

where $\boldsymbol{f}$ represents the body force vector, and where $\tilde{p}$ is a homogenized representation of the non-local accumulated plastic strain of the matrix material. This set of equations can be solved using a weak finite element form combined to a Newton-Raphson linearization procedure, see Wu et al. (2012) for details.

During that time interval, the known data are the macro-total strain tensor $\bar{\boldsymbol{\varepsilon}}_n$, the macro–strain increment $\Delta\bar{\boldsymbol{\varepsilon}}_{n+1}$ and the internal variables at t_n, which include the usual internal variables of the constituents material models and the residual variables computed from the elastic unloading step: the residual strains in the composite, in the inclusions phase, in the matrix phase and the residual stresses in the inclusions and matrix phases. The strain increment $\Delta\bar{\boldsymbol{\varepsilon}}_{n+1}$ resulting from the iterations at the weak form level is different from the strain increment $\Delta\bar{\boldsymbol{\varepsilon}}^{\mathrm{r}}_{n+1}$ applied to the LCC used in the MFH procedure. Combining (5) and (6) for the homogenized material, one has

$$\Delta\bar{\boldsymbol{\varepsilon}}^{\mathrm{r}}_{n+1} = \bar{\boldsymbol{\varepsilon}}_n + \Delta\bar{\boldsymbol{\varepsilon}}_{n+1} - \bar{\boldsymbol{\varepsilon}}^{\mathrm{res}}_n \,. \tag{55}$$

The explicit evaluation of $\bar{\boldsymbol{\varepsilon}}^{\mathrm{res}}_n$ is described in the details of the MFH process reported here below. Thus, based on the definition of $\boldsymbol{C}^{\mathrm{SD}}$ (52) for damage-enhanced elasto–plastic materials, the operators $\bar{\boldsymbol{C}}^{\mathrm{LCC}}_0$ and $\bar{\boldsymbol{C}}^{\mathrm{LCC}}_{\mathrm{I}}$ of the LCCs can be defined to apply the MFH scheme stated by Eqs. (1), (2) and (3). Eventually, the MFH process is summarized by the following equations

$$\begin{aligned}
\Delta\bar{\boldsymbol{\varepsilon}}^{\mathrm{r}}_{n+1} &= v_0\Delta\boldsymbol{\varepsilon}^{\mathrm{r}}_{0n+1} + v_{\mathrm{I}}\Delta\boldsymbol{\varepsilon}^{\mathrm{r}}_{\mathrm{I}n+1} \,, && (56)\\
\bar{\boldsymbol{\sigma}}_{n+1} &= v_0\boldsymbol{\sigma}_{0n+1} + v_{\mathrm{I}}\boldsymbol{\sigma}_{\mathrm{I}n+1} \,, && (57)\\
\Delta\boldsymbol{\varepsilon}^{\mathrm{r}}_{\mathrm{I}n+1} &= \boldsymbol{B}^{\epsilon}(\boldsymbol{I}, \bar{\boldsymbol{C}}^{\mathrm{SD}}_0, \bar{\boldsymbol{C}}^{\mathrm{S}}_{\mathrm{I}}) : \Delta\boldsymbol{\varepsilon}^{\mathrm{r}}_{0n+1} \,, && (58)
\end{aligned}$$

where the stress tensors are evaluated in each phase following Eq. (51), without damage for the inclusions phase. To complete this set, at the unloaded state, we have

$$\bar{\boldsymbol{\sigma}}^{\mathrm{res}}_n = v_0{\boldsymbol{\sigma}_0^{\mathrm{res}}}_n + v_{\mathrm{I}}{\boldsymbol{\sigma}_{\mathrm{I}}^{\mathrm{res}}}_n = 0 \,. \tag{59}$$

In this paper, a "first-order moment" method is considered, and the MFH process is described as follows. Note that during the MFH process, the strain increment of the composite $\Delta\bar{\boldsymbol{\varepsilon}}_{n+1}$, and the non–local plastic strain increment of the matrix $\Delta\tilde{p}_{n+1}$ – required to evaluate the damage – are constant, as they result from the FE iterations formulated from the strong form (53-54).

Practically, the resolution of Eqs. (55-59) is achieved as follows

- Initialize the strain increment in the inclusions phase: $\Delta\bar{\boldsymbol{\varepsilon}}^{\mathrm{r}}_{n+1} \rightarrow \Delta\boldsymbol{\varepsilon}^{\mathrm{r}}_{\mathrm{I}n+1}$.
- Follow the iterations process (upper indices (i) for values at iteration i of time t_{n+1} are omitted for simplicity):
    1. Call the constitutive material function of the real inclusions material with the strain tensor increment in the inclusions phase $\Delta\boldsymbol{\varepsilon}^{\mathrm{r}}_{\mathrm{I}n+1}$ and the internal variables at time t_n as input. After having applied the constitutive model described in Section 3.2, but without considering damage, the output is the updated stress $\boldsymbol{\sigma}_{\mathrm{I}n+1}$, the internal variables at time t_{n+1}, the "consistent"[3] (anisotropic) operator $\bar{\boldsymbol{C}}^{\mathrm{alg}}_{\mathrm{I}\ n+1} = \frac{\partial\boldsymbol{\sigma}_{\mathrm{I}n+1}}{\partial\Delta\boldsymbol{\varepsilon}_{\mathrm{I}n+1}}$[4], see Appendix C for details, and the incremental–secant operator $\bar{\boldsymbol{C}}^{\mathrm{S}}_{\mathrm{I}\,n+1}$ for the inclusions phase. In case there is no plastic flow, we use $\bar{\boldsymbol{C}}^{\mathrm{S}}_{\mathrm{I}\,n+1} = \boldsymbol{C}^{\mathrm{el}}_{\mathrm{I}}$.
    2. Compute the average strain in the matrix phase:
    $$\Delta\boldsymbol{\varepsilon}^{\mathrm{r}}_{0n+1} = (\Delta\bar{\boldsymbol{\varepsilon}}^{\mathrm{r}}_{n+1} - v_{\mathrm{I}}\Delta\boldsymbol{\varepsilon}^{\mathrm{r}}_{\mathrm{I}n+1})/v_0\,. \tag{60}$$
    3. Call the constitutive material function of the real matrix material with the strain tensor increment in the matrix phase $\Delta\boldsymbol{\varepsilon}^{\mathrm{r}}_{0n+1}$ and the internal variables at time t_n as input. After having applied the constitutive model described in Section 3.2, the output is the updated stress $\boldsymbol{\sigma}_{0n+1}$, the damage D_{n+1}, the internal variables at time t_{n+1}, the "consistent" (anisotropic) operators $\bar{\boldsymbol{C}}^{\mathrm{alg}}_{0\ n+1}$ and $\bar{\boldsymbol{C}}^{\mathrm{algD}}_{0\ n+1} = (1-D_{n+1})\,\bar{\boldsymbol{C}}^{\mathrm{alg}}_{0\ n+1}$, see Appendix C for details, and the incremental–secant operator $\bar{\boldsymbol{C}}^{\mathrm{SD}}_{0\ n+1}$ for the matrix phase. In case there is no plastic flow, we use $\bar{\boldsymbol{C}}^{\mathrm{SD}}_{0\ n+1} = (1-D_{n+1})\,\boldsymbol{C}^{\mathrm{el}}_{0}$.
    4. Predict the Eshelby tensor $\boldsymbol{S}(\boldsymbol{I}, \bar{\boldsymbol{C}}^{\mathrm{SD}}_{0\ n+1})$ using the isotropic damaged secant–operator of the matrix phase.
    5. For a time interval $[t_n,\, t_{n+1}]$ both $\Delta\bar{\boldsymbol{\varepsilon}}^{\mathrm{r}}_{n+1}$ and $\Delta\tilde{p}_{n+1}$ are constant and verifying Eq. (58) corresponds to satisfying $\boldsymbol{F} = 0$, where $\boldsymbol{F}$ is the stress residual vector developed in Appendix D, which

[3] In this paper we will use the term "consistent" operator for the derivative of the stress state with respect to the deformation increment

[4] The derivative with respect to $\Delta\boldsymbol{\varepsilon}^{\mathrm{r}}_{\mathrm{I}n+1}$ is the same as the derivative with respect to $\Delta\boldsymbol{\varepsilon}_{\mathrm{I}n+1}$

reads

$$\begin{aligned} \boldsymbol{F} &= \bar{\boldsymbol{C}}_{0\ n+1}^{\mathrm{SD}} : [\Delta\boldsymbol{\varepsilon}_{\mathrm{I}n+1}^{\mathrm{r}} - \frac{1}{v_0}\boldsymbol{S}^{-1} : (\Delta\boldsymbol{\varepsilon}_{\mathrm{I}n+1}^{\mathrm{r}} - \Delta\bar{\boldsymbol{\varepsilon}}_{n+1}^{\mathrm{r}})] \\ &\quad -\bar{\boldsymbol{C}}_{\mathrm{I}\ n+1}^{\mathrm{S}} : \Delta\boldsymbol{\varepsilon}_{\mathrm{I}n+1}^{\mathrm{r}} \,. \end{aligned} \tag{61}$$

6. Check if the residual $|\boldsymbol{F}| \leq \mathrm{Tol}$. If so exit the loop.
7. Else, compute the Jacobian matrix at constant $\Delta\bar{\boldsymbol{\varepsilon}}_{n+1}^{\mathrm{r}}$, such that $\mathrm{d}\boldsymbol{F} = \boldsymbol{J} : \mathrm{d}\boldsymbol{\varepsilon}_{\mathrm{I}}^{\mathrm{r}}$[5] following Appendix D.
8. Correct the strain increment in inclusions

$$\Delta\boldsymbol{\varepsilon}_{\mathrm{I}n+1}^{\mathrm{r}} \leftarrow \Delta\boldsymbol{\varepsilon}_{\mathrm{I}n+1}^{\mathrm{r}} + \boldsymbol{c}_{\boldsymbol{\varepsilon}_{\mathrm{I}}} \ \text{ with } \boldsymbol{c}_{\boldsymbol{\varepsilon}_{\mathrm{I}}} = -\boldsymbol{J}^{-1} : \boldsymbol{F} \,, \tag{62}$$

then start a new iteration (go to step 1).

- After convergence, compute
  1. The homogenized stress

$$\bar{\boldsymbol{\sigma}}_{n+1} = v_0\boldsymbol{\sigma}_{0n+1} + v_{\mathrm{I}}\boldsymbol{\sigma}_{\mathrm{I}n+1} \,, \tag{63}$$

  and the internal variables.
  2. The "consistent" linearization of the homogenized stress

$$\delta\bar{\boldsymbol{\sigma}} \;=\; \bar{\boldsymbol{C}}^{\mathrm{alg}} : \delta\bar{\boldsymbol{\varepsilon}} + \boldsymbol{C}_{\tilde{p}}\delta\tilde{p} \,, \tag{64}$$

  with the "consistent" tangent operators $\bar{\boldsymbol{C}}^{\mathrm{alg}}$ and $\boldsymbol{C}_{\tilde{p}}$ given in Appendix E.

- An unloading step is thus applied here to fit the incremental–secant process, and the obtained results will be kept as history variables at time step t_{n+1}. The required residual variables from unloading are the residual strains in the composite $\bar{\boldsymbol{\varepsilon}}_{n+1}^{\mathrm{res}}$, in the inclusions phase $\boldsymbol{\varepsilon}_{\mathrm{I}\ n+1}^{\mathrm{res}}$ and in the matrix phase $\boldsymbol{\varepsilon}_{0\ n+1}^{\mathrm{res}}$, as well as the residual stress in the inclusions phase $\boldsymbol{\sigma}_{\mathrm{I}\ n+1}^{\mathrm{res}}$ and the effective residual stress in the matrix phase $\hat{\boldsymbol{\sigma}}_{0\ n+1}^{\mathrm{res}}$, respectively.

[5] Note that the derivative with respect to $\Delta\boldsymbol{\varepsilon}_r^{\mathrm{r}}$ has the same expression as the derivative with respect to $\boldsymbol{\varepsilon}_r$ for a phase r

1. The residual strain $\bar{\boldsymbol{\varepsilon}}^{\mathrm{res}}_{n+1}$ (the strain at $\bar{\boldsymbol{\sigma}}^{\mathrm{res}}_{n+1}=0$) of the composite is calculated from an unloading step, which is assumed to be a purely elastic process. The unloading operator of the damaged composite is

$$\begin{aligned}\bar{\boldsymbol{C}}^{\mathrm{elD}}_{n+1} &= \left[v_{\mathrm{I}}\boldsymbol{C}^{\mathrm{el}}_{\mathrm{I}\,n+1} : \boldsymbol{B}^{\epsilon} + v_0 \boldsymbol{C}^{\mathrm{elD}}_{0\;n+1}\right] : \left[v_{\mathrm{I}}\boldsymbol{B}^{\epsilon} + v_0\boldsymbol{I}\right]^{-1}, \qquad (65)\\ \text{with}\\ \boldsymbol{B}^{\epsilon} &= \left\{\boldsymbol{I} + \boldsymbol{S} : \left[\left((1-D_{n+1})\,\boldsymbol{C}^{\mathrm{el}}_{0\,n+1}\right)^{-1} : \boldsymbol{C}^{\mathrm{el}}_{\mathrm{I}\,n+1} - \boldsymbol{I}\right]\right\}^{-1}. \qquad (66)\end{aligned}$$

   Note that $\boldsymbol{C}^{\mathrm{elD}}_{0\;n+1} = (1-D_{n+1})\,\boldsymbol{C}^{\mathrm{el}}_{0\,n+1}$ is used in the Eshelby tensor of the elastic unloading step. The residual strain of the composite satisfying (59) can be calculated by

$$\begin{aligned}\bar{\boldsymbol{\varepsilon}}^{\mathrm{res}}_{n+1} &= \bar{\boldsymbol{\varepsilon}}_{n+1} - \Delta\bar{\boldsymbol{\varepsilon}}^{\mathrm{unload}}_{n+1}\\ &= \bar{\boldsymbol{\varepsilon}}_{n+1} - (\bar{\boldsymbol{C}}^{\mathrm{elD}}_{n+1})^{-1} : \bar{\boldsymbol{\sigma}}_{n+1}. \qquad (67)\end{aligned}$$

2. The residual strains in the inclusions and in the matrix phases are computed following the M-T method, yielding

$$\begin{aligned}\boldsymbol{\varepsilon}^{\mathrm{res}}_{\mathrm{I}\;n+1} &= \boldsymbol{\varepsilon}_{\mathrm{I}n+1} - \Delta\boldsymbol{\varepsilon}^{\mathrm{unload}}_{\mathrm{I}\;n+1}\\ &= \boldsymbol{\varepsilon}_{\mathrm{I}n+1} - \boldsymbol{B}^{\epsilon} : \left[v_{\mathrm{I}}\boldsymbol{B}^{\epsilon} + v_0\boldsymbol{I}\right]^{-1} : \Delta\bar{\boldsymbol{\varepsilon}}^{\mathrm{unload}}_{n+1}, \qquad (68)\\ \varepsilon^{\mathrm{res}}_{0\;n+1} &= \varepsilon_{0n+1} - \Delta\varepsilon^{\mathrm{unload}}_{0\;n+1}\\ &= \varepsilon_{0n+1} - \left[v_{\mathrm{I}}\boldsymbol{B}^{\epsilon} + v_0\boldsymbol{I}\right]^{-1} : \Delta\bar{\boldsymbol{\varepsilon}}^{\mathrm{unload}}_{n+1}. \qquad (69)\end{aligned}$$

3. The residual (effective) stresses in the inclusions and matrix phases can be obtained, respectively, from

$$\boldsymbol{\sigma}^{\mathrm{res}}_{\mathrm{I}\;n+1} = \boldsymbol{\sigma}_{\mathrm{I}n+1} - \boldsymbol{C}^{\mathrm{el}}_{\mathrm{I}\,n+1} : \Delta\boldsymbol{\varepsilon}^{\mathrm{unload}}_{\mathrm{I}\;n+1}, \qquad (70)$$

$$\hat{\boldsymbol{\sigma}}^{\mathrm{res}}_{0\;n+1} = \hat{\boldsymbol{\sigma}}_{0\,n+1} - \boldsymbol{C}^{\mathrm{el}}_{0\,n+1} : \Delta\boldsymbol{\varepsilon}^{\mathrm{unload}}_{0\;n+1}. \qquad (71)$$

Note that by expressing Eqs. (67-69) at time t_n, one has

$$\bar{\boldsymbol{\varepsilon}}^{\mathrm{res}}_{n} = v_0\boldsymbol{\varepsilon}^{\mathrm{res}}_{0\;n} + v_{\mathrm{I}}\boldsymbol{\varepsilon}^{\mathrm{res}}_{\mathrm{I}\;n}. \qquad (72)$$

Moreover, Eqs. (55) and (56) yield

$$v_0\Delta\boldsymbol{\varepsilon}^{\mathrm{r}}_{0n+1} + v_{\mathrm{I}}\Delta\boldsymbol{\varepsilon}^{\mathrm{r}}_{\mathrm{I}n+1} = \Delta\bar{\boldsymbol{\varepsilon}}^{\mathrm{r}}_{n+1} = v_0\boldsymbol{\varepsilon}_{0n} + v_{\mathrm{I}}\boldsymbol{\varepsilon}_{\mathrm{I}n} + \Delta\bar{\boldsymbol{\varepsilon}}_{n+1} - \bar{\boldsymbol{\varepsilon}}^{\mathrm{res}}_{n}, \qquad (73)$$

which becomes, after using Eq. (72),

$$\Delta\bar{\boldsymbol{\varepsilon}}_{n+1} = v_0 \left(\Delta\boldsymbol{\varepsilon}^{\mathrm{r}}_{0n+1} - \boldsymbol{\varepsilon}_{0n} + {\boldsymbol{\varepsilon}_0^{\mathrm{res}}}_n\right) + v_{\mathrm{I}} \left(\Delta\boldsymbol{\varepsilon}^{\mathrm{r}}_{\mathrm{I}n+1} - \boldsymbol{\varepsilon}_{\mathrm{I}n} + {\boldsymbol{\varepsilon}_{\mathrm{I}}^{\mathrm{res}}}_n\right) . \tag{74}$$

This relation demonstrates that the process still satisfies

$$\Delta\bar{\boldsymbol{\varepsilon}}_{n+1} = v_0 \Delta\boldsymbol{\varepsilon}_{0n+1} + v_{\mathrm{I}} \Delta\boldsymbol{\varepsilon}_{\mathrm{I}n+1} . \tag{75}$$

These relations can be used in a FE implementation. More details about the FE implementation of a non-local MFH were discussed by Wu et al. (2012) for an incremental–tangent approach, and can be directly adapted for this incremental–secant approach.

4. Model validation

In this section, the accuracy and the reliability of the proposed incremental–secant method with non–local damage are first assessed through the comparison with direct FE simulations on representative unit cells of the micro-structure. In particular it is shown that the new incremental–secant MFH method reaches a higher accuracy than the incremental–tangent MFH scheme previously developed by Wu et al. (2012). The model is then validated against experimental results for a metallic composite material.

4.1. Comparison with direct FE simulations

The example studied by Wu et al. (2012), using an incremental–tangent MFH and with FE simulations of a periodical cell, is considered herein. This consists of continuous elastic isotropic fibers embedded in a matrix material, which follows the elasto–plastic behavior model enhanced by a non-local damage setting, as described in Section 3.1. The material parameters are

- Inclusions: $E_{\mathrm{I}} = 238\mathrm{GPa}$, $\nu_{\mathrm{I}} = 0.26$.
- Matrix: $E_0 = 2.89\mathrm{GPa}$, $\nu_0 = 0.3$, $\sigma_{Y0} = 35\mathrm{MPa}$, $h_0 = 73\mathrm{MPa}$, $m_0 = 60$, $S_0 = 2\mathrm{MPa}$, $s = 0.5$ and $p_C = 0$,

which follows the hardening law (76)

$$R_0(p) = h_0 \left(1 - e^{-m_0 p}\right) , \tag{76}$$

and the damage law (21). The volume fraction of the continuous fibers is $v_{\mathrm{I}} = 50\%$. The test consists in a transverse loading of the composite under

constrained strain (with plane–stress state in the other transverse direction and plane–strain state in the longitudinal direction), followed by a complete unloading until reaching a zero-strain state. As the inclusions remain elastic, the matrix obeys to the zero–incremental–secant formulation while the inclusions phase follows the residual–incremental–secant formulation. For the FE cell simulations, the characteristic length of the matrix phase is taken such that $l^2 = 2$ mm^2. This value was calibrated from experimental results by Geers et al. (1999) for short fiber composites and is used herein for the matrix phase. For the MFH results, as the fields remain uniform, the results are independent on this characteristic length.

Figures 5(a) and 5(b) compare the macro–stress evolution, respectively along the loading direction and along the fibers direction, obtained with the new incremental–secant MFH and the previously developed incremental–tangent MFH to the FE results. Clearly, the tangent method overestimates the results. This is in agreement with what was stated by Wu et al. (2012): the accuracy of the incremental–tangent method decreases after strain softening of the matrix as the fibers cannot see the elastic unloading which should arise due to the damaging process in the matrix. This is clearly illustrated in Fig. 5(c) where the average stress along the loading direction in the fibers keeps increasing during the loading process. As expected, the new method does not suffer from this limitation: the fibers are unloaded during the softening process, see Fig. 5(c), and the method predicts the macro-stress with a higher accuracy, see Fig. 5(a). The average stress state in the matrix is also predicted with a better accuracy as shown in Fig. 5(d).

Figure 5(e) compares the average value of the effective equivalent von Mises stress in the matrix. For the FE simulations, the value is obtained by averaging the effective von Mises stress computed at each integration point. For the first–order MFH schemes, by definition, this value is obtained as the equivalent von Mises value of the average effective stress tensor in the matrix. Results obtained by the three methods are comparable during the plastic flow, except during the unloading in the vicinity of the point at which the composite stress along the loading direction vanishes. At that stage, the stresses in the matrix and in the fibers phases are close to zero for the FE simulations and for the incremental–secant MFH. As a consequence the effective von Mises stress in the matrix phase predicted by the incremental–secant MFH is also close to zero. As the stress distribution in the matrix phase of the direct FE simulation is not uniform –parts are in tension and parts are in compression, the average of the matrix average effective von Mises

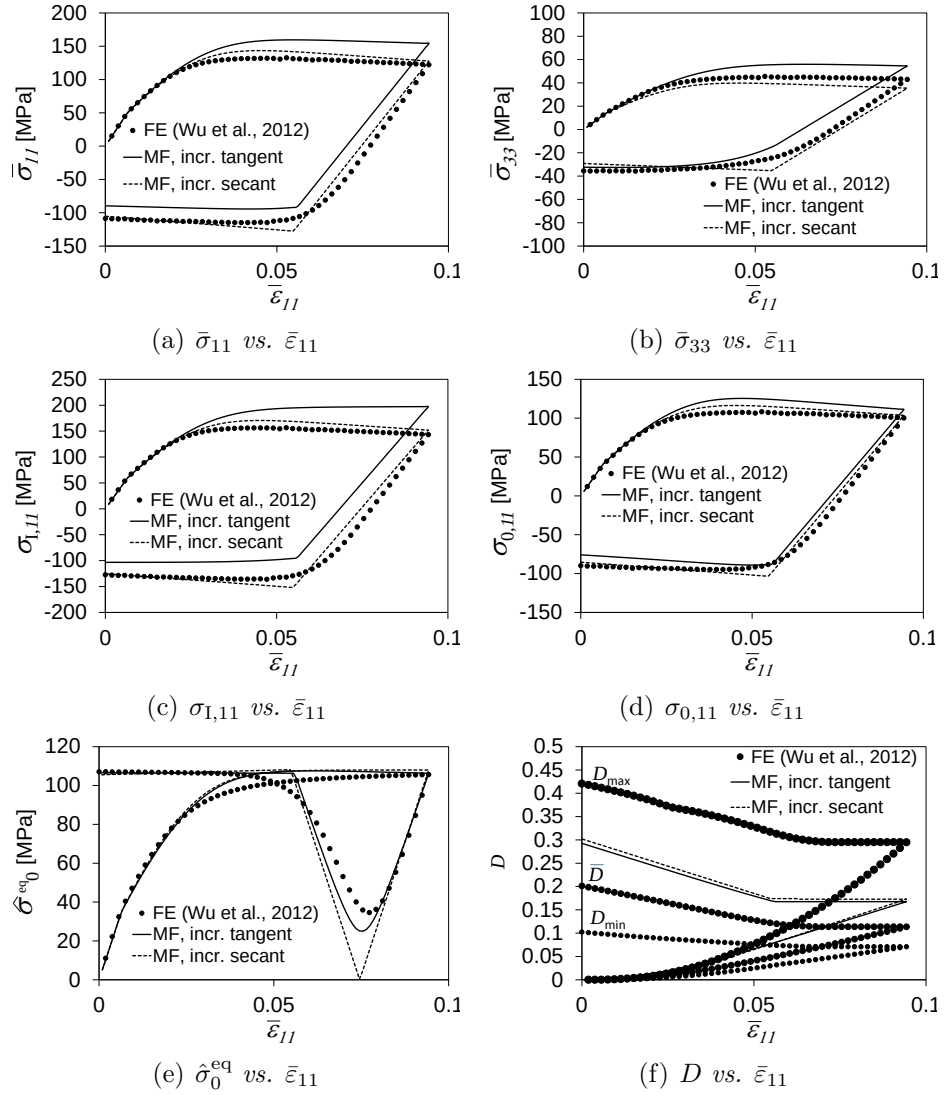

(a) $\bar{\sigma}_{11}$ *vs.* $\bar{\varepsilon}_{11}$ (b) $\bar{\sigma}_{33}$ *vs.* $\bar{\varepsilon}_{11}$

(c) $\sigma_{\mathrm{I},11}$ *vs.* $\bar{\varepsilon}_{11}$ (d) $\sigma_{0,11}$ *vs.* $\bar{\varepsilon}_{11}$

(e) $\hat{\sigma}_0^{\mathrm{eq}}$ *vs.* $\bar{\varepsilon}_{11}$ (f) D *vs.* $\bar{\varepsilon}_{11}$

Figure 5: Results for continuous-elastic fibers embedded in a matrix following an elasto–plastic behavior with damage. Comparison of the values obtained with the direct FE simulations and with the MFH schemes. (a, b) Average stresses in the composite material along the loading direction and along the fiber direction. (c, d) Average stresses in both phases along the loading direction. (e) Effective von Mises stress in the matrix phase. (f) Damage in the matrix phase –the minimum, average, and maximum damage values are reported.

stress is never equal to zero. This is a limit of the first–order method as

$\langle \boldsymbol{\sigma}^{\mathrm{eq}} \rangle_{\omega_0} \neq \left(\langle \boldsymbol{\sigma} \rangle_{\omega_0} \right)^{\mathrm{eq}}$. Note that results obtained by the incremental–tangent MFH are actually not more accurate. Indeed in the vicinity of the point at which the composite stress along the loading direction vanishes, the average stress along the fibers direction is overvalued with the incremental–tangent method, see Fig. 5(b), which explains why the von Mises stress in the matrix does not vanish. This is actually due to the unability of the incremental method to consider non–monotonic loadings as shown by Wu et al. (Submitted).

Finally, Fig. 5(f) illustrates the damage evolution in the matrix. For the FE prediction, the minimum, average and maximum values of the damage reached in the matrix are reported. It can be seen that the damage predicted by the MFH methods lies between the average and maximum damage predicted by the FE simulations. This comes from our definition of the damage of the MFH, which does not correspond to the average damage. During the decrease of the strain to zero, the composite material is first unloaded and then enters into compression. This compression induces an increase of the accumulated plastic strain and of the damage.

4.2. Comparison with experimental results

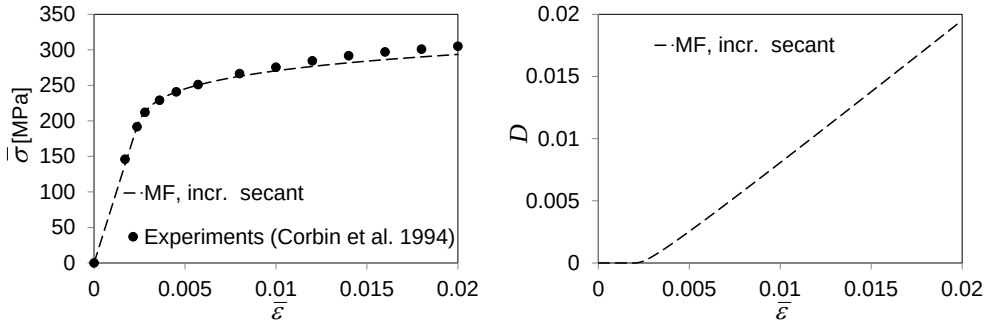

(a) Stress (b) Damage

Figure 6: SiC particles–reinforced AL–Si–Mg alloy. (a) Comparison between the damage-enhanced MFH prediction and the experimental results. (b) Damage evolution predicted in the matrix.

The presented model is now applied to predict the macro-mechanical response of a metal matrix composite material in tension. The considered material consists of SiC particles–reinforced AL–Si–Mg alloy (A356) with T61 ageing. The experimental results presented by Corbin and Wilkinson (1994)

are used as the reference. The SiC spherical particules are modeled with a linear elastic material without damage and their properties were reported by Christman et al. (1989). The constitutive equation of the matrix material follows a Ramburg–Osgood equation,

$$\varepsilon = \frac{\sigma}{E} + \alpha \frac{\sigma_0}{E} (\frac{\sigma}{\sigma_0})^{1/N} , \tag{77}$$

where $\alpha \frac{\sigma_0}{E} = 0.002$ according to the definition of the yielding stress, E the is elastic modulus, σ_0 is the yield strength defined at an offset of 0.2%, and where N is the strain hardening exponent. The matrix material experiences a linear plastic damage evolution according to the experimental result obtained by Corbin and Wilkinson (1994) on the un–reinforced A356–T61 alloy. The material parameters are

- Inclusions: $E_{\mathrm{I}} = 450\mathrm{GPa}$, $\nu_{\mathrm{I}} = 0.17$.
- Matrix: $E_0 = 70\mathrm{GPa}$, $\nu_0 = 0.33$, $\sigma_0 = 220\mathrm{MPa}$, $N = 0.1$, and damage law $D = 0.875p$,

where p is the accumulated plastic strain and where the damage evolution law is obtained through a curve fitting of the experimental data reported by Corbin and Wilkinson (1994) (Fig. 7 of this reference).

The resulting experimental data obtained by Corbin and Wilkinson (1994) for a uni-axial tension on a material with $v_I = 10\%$ volume fraction of spherical inclusions are compared to the results obtained by the the presented MFH model in Fig. 4.2, where a good agreement can be seen. The damage evolution in the matrix predicted by the homogenization model is illustrated in Fig. 4.2. Note that in our model we assume that the particles are uniformly distributed, which is not always the case in real materials but remains reasonable for $v_I = 10\%$ volume fraction of inclusions.

5. Applications

In this section, the developed non-local MFH model is applied to study meso- and macro–scale problems. At first the convergence of the method with respect to the mesh size upon strain softening is demonstrated on a notched composite ply. Then, a composite laminate is studied. In a first set of studies the predictions of the damage–enhanced MFH model are compared with experimental results on coupon tensile tests. These tests include an

unloading stage to validate the damage model. Then the same laminate is used on a specimen with a hole. In this last example it can be seen that the damage–enhanced MFH captures the damage path oriented along the fibers directions in each ply, accordingly to experimental results.

5.1. Notched sample

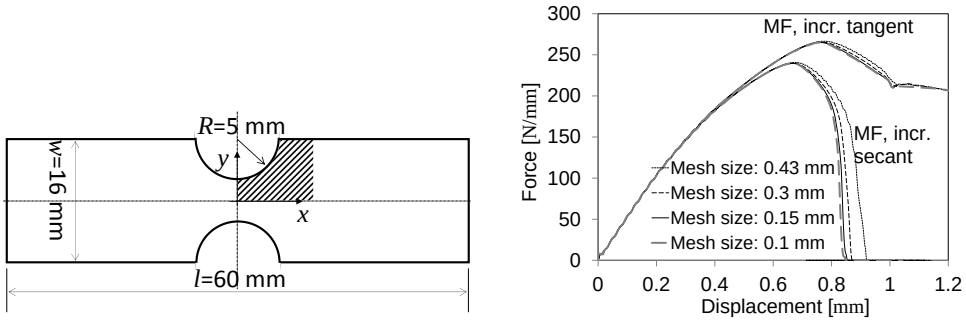

(a) Schematics (b) Response

Figure 7: Sample with a notch. (a) Schematics of the sample test. (b) Force per unit ply length vs. displacement of the sample for different meshes.

In this section, the two-dimensional example proposed by Wu et al. (2012), the authors, to study the convergence of the non-local damage–enhanced MFH method with respect to the mesh size, is considered. In particular the effect of the mesh size upon strain softening is analyzed using the developed incremental–secant MFH formulation. Results are also compared to the ones previously obtained by Wu et al. (2012) with the incremental–tangent MFH method.

The specimen, whose geometry is illustrated in Fig. 7(a), represents the transverse section of a unidirectional reinforced ply. In order to study the effect of the non-local damage model, notches are added to force strain localization. The same material system as in Section 4.1 is considered herein but with a fiber volume ratio $v_{\mathrm{I}} = 0.3$ and with the characteristic length $l^2 = 2.0$ mm^2. It should be noted that these values are the ones studied by Wu et al. (2012) for comparison purpose. The fibers are assumed to be perpendicular to this section. Thus plane-strain conditions are applied in the fiber direction (z–direction), and traction-free conditions are applied along the ply-thickness (y–direction).

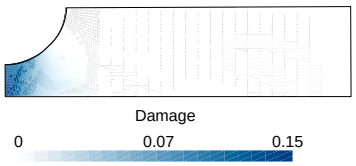

(a) Incremental–secant, strain softening onset

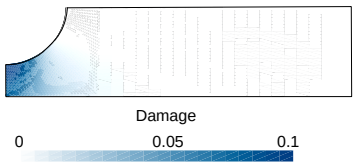

(b) Incremental–tangent, strain softening onset

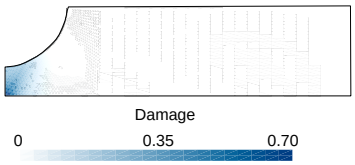

(c) Incremental–secant, 0.825 mm–displacement

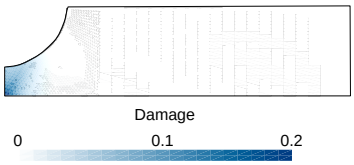

(d) Incremental–tangent, 0.825 mm–displacement

Figure 8: The damage distribution in the matrix phase for the mesh –mesh size=0.15 mm– obtained at (a-b) strain softening onset, (c-d) 0.825 mm–displacement, and with the (a), (c) incremental–secant MFH scheme, (b), (d) incremental–tangent MFH scheme.

Because of the symmetry, only one quarter of the structure is considered in the finite element simulations. The mesh of the quarter specimen is refined in the weak zone of 8.0×8.0 mm (see the shadow area in Fig. 7(a)), and four meshes are successively considered:

- Coarsest mesh of 182 elements and with a mesh size of about 0.43 mm at the notch ;
- Intermediate mesh of 360 elements and with a mesh size of about 0.3 mm at the notch;
- Fine mesh of 1120 elements and with a the mesh size of about 0.15 mm at the notch.
- Finest mesh of 2540 elements and with a the mesh size of about 0.1 mm at the notch.

Bi–linear quadrangular elements with locking control are used.

The load-displacement curves are extracted for the four mesh sizes and are presented in Fig. 7(b). When considering both the incremental–tangent and the incremental–secant MFH, a good convergence can be seen with the

decrease of the mesh size. Indeed, the difference between the curves for mesh sizes of 0.15 mm and 0.3 mm is much smaller than the difference between the curves for mesh sizes of 0.3 mm and 0.43 mm, despite a larger difference in the mesh reduction. The results for a mesh–size of 0.1 mm are ever closer to the 0.15 mm mesh–size curve.

As expected, with the incremental–tangent MFH scheme the predicted strain softening onset is over–estimated compared to the results obtained with the incremental–secant MFH method, which allows the fibers to be unloaded during the damaging process. Also with the incremental–tangent method, during the softening part for a displacement close to 1 mm, the matrix phase is totally unloaded but not the inclusion phase explaining the kink. The incremental–secant method does not suffer from the limitation and allows a complete unloading of the homogenized material to be achieved.

This stress overestimation predicted by the incremental–tangent method is also observed when analyzing the matrix damage distributions obtained for the finest mesh with the two methods at strain softening onset, Figs. 8(a) and 8(b), and at the maximum displacement reached (0.825 mm), Figs. 8(c) and 8(d). The damage reached with the incremental–secant method is higher than with the incremental–tangent method, especially during the strain softening part of the curve.

5.2. Tensile tests on laminates

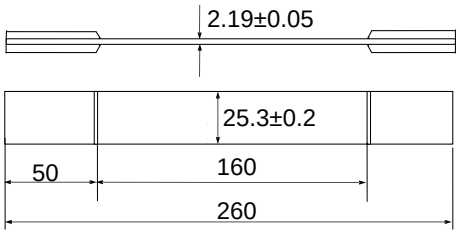

Figure 9: Geometry schematics of the tensile specimens (units in mm).

In this section, the anisotropic gradient enhanced MFH model is used to investigate the response of laminates made of a unidirectional (UD) $[-45^o_2 \,/\, 45^o_2]_S$ stacking sequence, and subjected to a uni–axial tension. The geometry of the sample is illustrated in Fig. 9.

In order to validate the damage model, experiments are conducted in

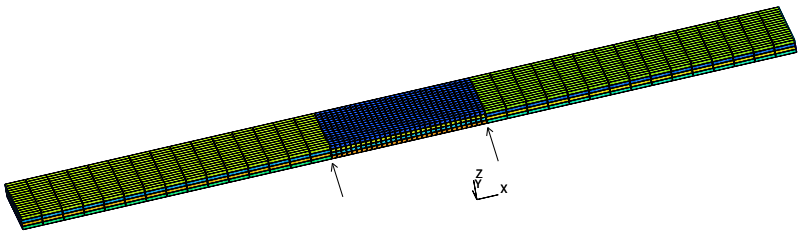

Figure 10: Mesh of the $[45^o_2/-45^o_2]_S$ laminate. Arrows indicate the grips of the extensometer.

which the samples are loaded up to 0.56%-strain[6] before being unloaded and then reloaded a second time to reach the same stress level. The specimens of carbon fibers reinforced epoxy composite are manufactured from prepreg Hexply M10.1/38%/UD300/HS (R), with a $[-45^o_2/45^o_2]_S$ stacking sequence. The total thickness of the specimens is 2.19±0.05 mm. After curing, the resulting fiber volume fraction is $\nu_{\mathrm{I}} = 60\%$[7]. The specimens are cut from an autoclave consolidated unidirectional laminate panel of 300×300 mm^2, and their geometry schematic is shown in Fig. 9. To prevent gripping damage, aluminum tabs are glued at both extremities of each specimen. The static tensile tests are carried out on a 1185 n^o H4573(ME002) Instran machine in displacement control mode with a constant cross–head speed of 2 mm/min, according to the specification of ISO–527–4 standard. An extensometer measures the average strain in the 50–mm band.

A numerical model is made by meshing the different plies of the laminate sample, and is illustrated in Fig. 10. Each ply orientation is meshed by 915 bi–linear quadrangular elements with locking control. In each ply, the MFH model is used as a material law with the proper fiber orientations. Constrained displacements are applied along the x–axis at both laminate extremities and the deformations are measured from the displacements at the nodes corresponding to the extensometer grips positions (arrows on Fig. 10) .

[6]Before failure of the specimens happens

[7]The percentage is a mean value obtained from a microscopic imaging process of the cured laminates

In this application, the following length scales are considered: $c^3 = 2.0$ mm^2 as suggested by Geers et al. (1999) for short fiber composites along the fiber directions, and $c^1 = c^2 = 8.45 \times 10^{-5}$ mm^2 in the transverse direction. In this direction $c^1 = c^2$ is equal to $\frac{l^2}{2}$, where l is the maximum distance of possible interaction between material points (Peerlings et al., 2001). In our case, this distance corresponds to the distance between fibers, which are obstacles to the interaction, and can be statistically computed from the volume fraction of fibers (60%) and from the fibers diameter (10 μm). Note that an artificial spreading of the damaged zone orthogonal to the direction of a possible crack propagation has been observed by Geers et al. (1998, 1999) in the numerical simulations involving damage to fracture transition with constant l, but this is beyond the scope of this paper.

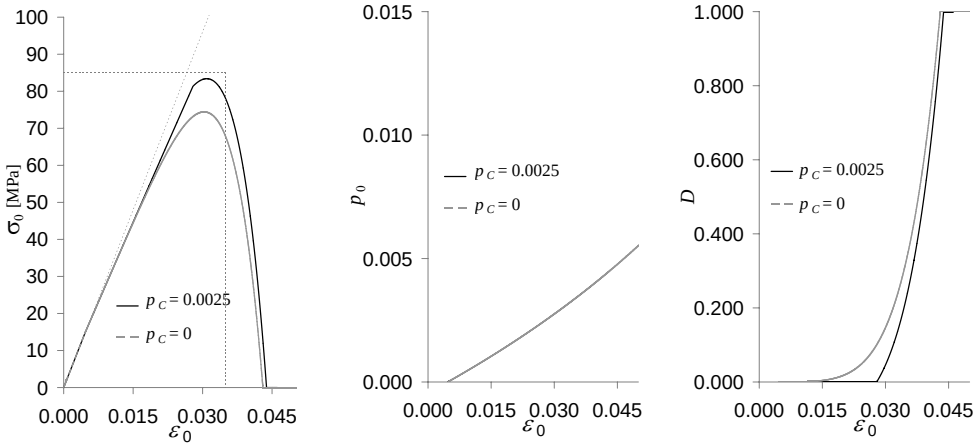

(a) Stress (b) Plastic strain (c) Damage

Figure 11: Tensile stress–strain results predicted with the considered elasto–plastic model with damage for the epoxy matrix. (a) Stress–strain curve, the linear response, the tensile strength, and the maximum tensile strain given by the manufacturer are reported in dotted lines. (b) Evolution of the accumulated plastic strain. (c) Evolution of the damage.

In order to conduct the numerical simulations, the material properties, of the different phases are identified as follows. The carbon fibers are assumed to be linear elastic and transversely isotropic. Typical material constants (Byström, 2009, *e.g*) for T300 carbon fibers are considered. The cured epoxy matrix properties reported by the manufacturer are a tensile modulus of 3.2 GPa, and a tensile strength of 85 MPa at 0.035–strain. By lack of elasto–

plastic data, an exponential hardening law (76) and a power damage law (21) are considered. The material properties used are thus

- Inclusions: Longitudinal Young modulus $E_{\mathrm{L}} = 230$ GPa, transverse Young modulus $E_{\mathrm{T}} = 40$ [GPa], transverse Poisson ratio $\nu_{\mathrm{TT}} = 0.20$, longitudinal–transverse Poisson ratio $\nu_{\mathrm{LT}} = 0.256$, transverse shear modulus $G_{\mathrm{TT}} = 16.7$ [GPa], longitudinal–transverse shear modulus $G_{\mathrm{LT}} = 24$ [GPa].

- Matrix: $E_0 = 3.2$GPa, $\nu_0 = 0.3$, $\sigma_{Y0} = 15$MPa, $h_0 = 300$MPa, $m_0 = 100$, $S_0 = 0.1$MPa, $s = 2$ and $p_C = 0$.

The corresponding stress–strain curve of the epoxy matrix is illustrated on Fig. 11(a), where the manufacturer data are also reported. With the considered law, it was not possible to reach the maximum stress at an exact 0.035–strain, and the maximum strain is reached during the softening part. Moreover, to account for the non–local framework for which the damage is computed from a non-local accumulated plastic strain, the matrix law was fitted using a damage threshold at p_C=0.0025 instead of the used value of 0. From the damage evolution on Fig. 11(c), it can be seen that softening onset is reached for a damage value around 0.032.

Five samples are tested and their stress-strain curves are compared to the numerical predictions. The first loading strain–stress curves and the curves extracted from the unloading/second loading[8] are reported in Figs. 12(a) and 12(b). It can be seen that the model is in excellent agreement with the experiments. In particular, the MFH model with damage allows predicting the unloading with a high accuracy, and the residual strain is in perfect agreement with the experiments, as it can be observed on Fig. 12(b).

Remark that for these tests, the values of the damage reached are low because the geometry is perfectly regular and because the non-local approach avoids spurious localization. For a real geometry the imperfection will cause a shear band. In order to demonstrate that the approach can initiate such a band we consider in the next section an application in which a strain gradient naturally exists.

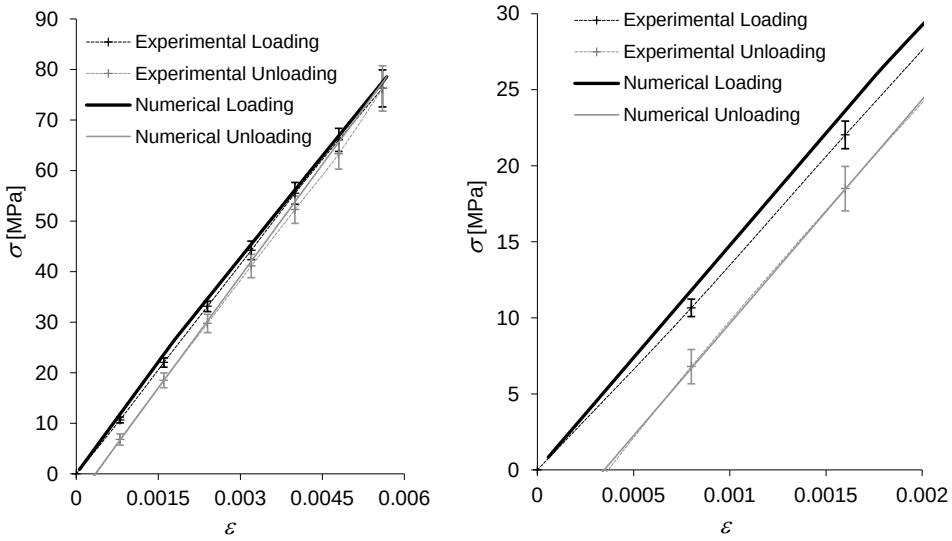

(a) Full curves (b) Zoom

Figure 12: Results for 60-% volume UD transverse-isotropic fibers reinforced epoxy tensile test with unloading and reloading on the $[45^o_2/-45^o_2]_S$ stacking sequence. The experimental strain corresponds to the average strain value measured by a 50–mm long extensometer. The average values obtained for the experimental tests are reported with their discrepancy range and are compared to the numerical curves.

5.3. Laminate with a hole

In the previous section, the localization of damage during the experiments was not controlled. In this section, the response of an open hole specimen made of the same UD $[-45^o_2/45^o_2]_S$ stacking sequence, and subjected to a uni–axial tension is studied. The presence of the hole allows a comparison of the localization effects happening during the experiments and predicted by the numerical model. The geometry of the sample is illustrated in Fig. 13(a). For the numerical model, although the plate is not symmetrical locally because of the material anisotropy, the global behavior is symmetrical on the width of the sample as the stacking sequence is balanced. Thus the numerical model considers only half of the plate, with 1280 x 8 elements, see Fig. 13(b).

[8] As during unloading dynamic effects affect the strain–stress curves, the classical method which consists in linearizing between the unloading and the second loading is used.

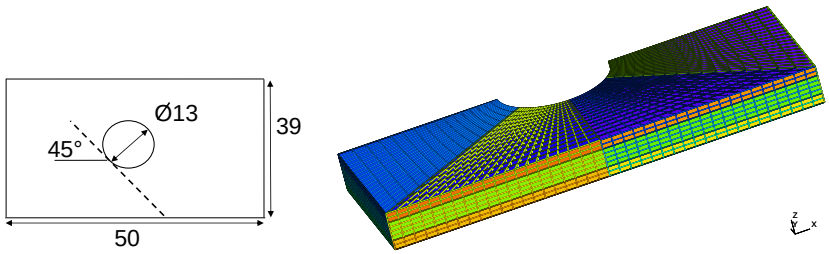

(a) Geometry (b) Mesh

Figure 13: Model of the $[-45^o_2/45^o_2]_S$–laminate with a hole. Units are expressed in mm, and the total thickness is 2.2 mm.

This approximation is valid as the local behavior of interest issues from the hole, which is not on the "pseudo" symmetrical axis. Bi–linear quadrangular elements with locking control are used.

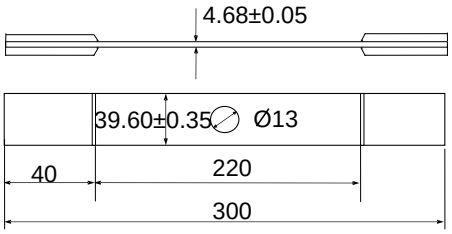

Figure 14: Geometry schematics of the specimens used during experiments.

In this application, the numerical and material parameters are identical as the ones reported in Section 5.2. The tests are conducted on specimens, whose geometry schematic is shown in Fig.14, manufactured as described in Section 5.2. The tensile tests also follows the same protocol.

Numerical predictions and experimental results are compared in Fig. 15(a). The stress evolution, evaluated by dividing the tensile load by the cross–section area, is in excellent agreement up to 0.2 % deformation. Upon this state the stress is over–predicted, with a maximum discrepancy near the fracture onset, see Fig. 15(a). The difference between the numerical prediction and the experimental results comes from the other damaging mechanisms such as delamination, fiber pull-out etc, which are not taken into account in the simulation. To illustrate this point we have also reported the solution predicted for independent plies on Fig. 15(a), meaning as if the plate was fully delaminated, and it can be seen that the experimental results get closer

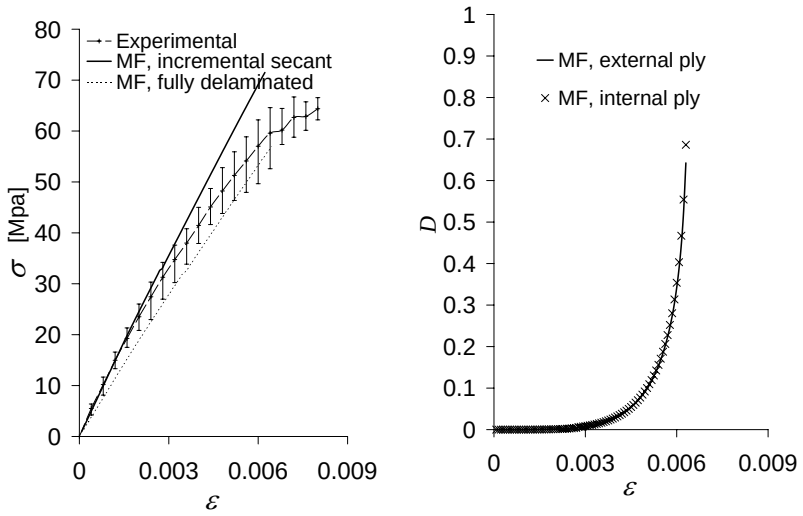

(a) Stress–strain curve (b) $D_{\max}$ in internal plies

Figure 15: Results for 60-% volume UD transverse-isotropic fibers reinforced epoxy tensile tests on the $[45_2^o/-45_2^o]_S$ stacking sequence with a hole. (a) Stress–strain curve. The experimental strain corresponds to the average strain value measured by a 50–mm long extensometer. We have also reported the solution predicted for independent plies, meaning as if the plate was fully delaminated. (b) Damage evolution in the internal and external plies.

from this last curve during the tensile tests. Finally the damage evolution is reported in Fig. 15(b), and Figs. 16 exhibit the damage distributions in the external and internal plies. It can be seen that the maximum damage location of the numerical predictions is in good agreement with the crack initiation location in the different plies observed for the experimental results, see Fig. 17. Moreover, the damage bands propagate along directions parallel to the fibers orientations and the damage reaches a value close to one when fracture is experimentally observed. Note that experimentally the cracks propagate with a -45–degree angle in the outer plies (Fig. 17) and with a 45–degree angle in the inner plies. These two orientations can be seen simultaneously in the numerical predictions under the form of damage bands in both the inner and in the outer plies (as the displacements are continuous at plies interfaces), see Fig. 16, but the high damage concentrations (close to one) follow the respective -45–degree direction in the outer plies, see Fig. 16(a), and the 45–degree direction in the inner plies, see Fig. 16(b).

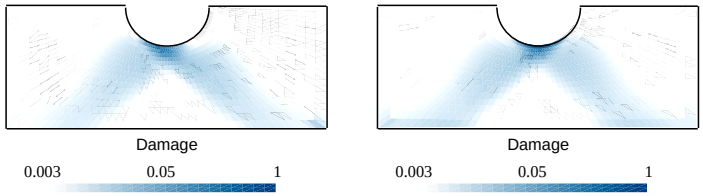

(a) External plies (b) Central plies

Figure 16: Snapshots of the damage distribution (logarithmic scale) for an average 0.65% strain (a) Outer ply, (b) Inner ply.

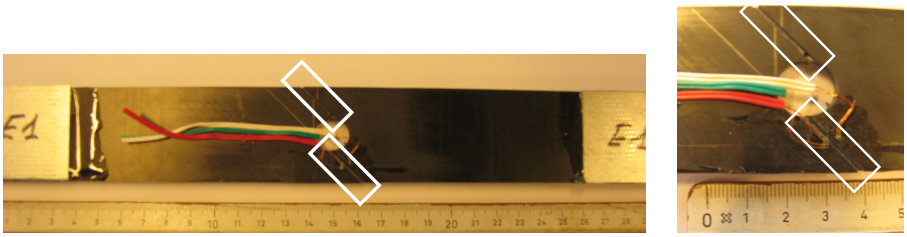

Figure 17: Broken open hole sample. The cracks follow the $\pm 45^o$–directions in each ply and originate from the predicted locations.

6. Conclusions

In this work, a new incremental–secant MFH process for composites made of elasto–plastic constituents exhibiting damage was proposed. In this approach, an unloading of the composite material is virtually performed to estimate the residual strains in each phase, before applying a secant approach on the strain increments, which differ in each phase. In order to define the LCC, two secant operators were defined. The first one, the residual–incremental–secant operator, is defined from the phase residual stress. The second operator, the zero–incremental–secant operator, is defined from a stress-free state in the phase.

The main advantage of this secant approach is made obvious when considering a composite whose matrix phase exhibits a damaging process. In this case, the inclusions phase can be unloaded during the softening stage of the matrix, ensuring an accurate prediction of the scheme. In particular, it was shown that for a composite with 50% volume ratio of fibers, the new incremental–secant–method is much more accurate than the incremental–tangent approach previously developed.

As classical FE formulations lose solution uniqueness and face the strain localization problem when strain softening of materials is involved, the model was formulated in a so-called implicit non–local approach. It was shown in a numerical example that the numerical simulations converges with the mesh size during the strain softening response.

Finally the model has been applied to study the response of laminates. First the material model has been validated by considering tensile tests including unloading on coupons. Then specimens made of the same laminate, but with a hole forcing the localization, have been considered. As a result we have a multiscale model that can predict the damage evolution in each ply of a composite stack. It was shown that the predicted damage evolution follows the fibers direction accordingly to the experimental results.

In the future it is intended to account for more degradation processes, such as delamination, but also to formulate the incremental–secant method in a second–moment framework to improve its accuracy even further.

Appendix A. Tensorial operations and notations

- Dots and colons are used to indicate tensor products contracted over one and two indices respectively:

$$\begin{aligned} \boldsymbol{u}\cdot\boldsymbol{v} &= u_i v_i, & (\boldsymbol{a}\cdot\boldsymbol{u})_i &= a_{ij}u_j\,; \\ (\boldsymbol{a}\cdot\boldsymbol{b})_{ij} &= a_{ik}b_{kj}, & \boldsymbol{a}:\boldsymbol{b} &= a_{ij}b_{ji}\,; \\ (\boldsymbol{C}:\boldsymbol{a})_{ij} &= C_{ijkl}a_{lk}, & (\boldsymbol{C}:\boldsymbol{D})_{ijkl} &= C_{ijmn}D_{nmkl}\,. \end{aligned} \tag{A.1}$$

- Dyadic products are designated by $\otimes$:

$$(\boldsymbol{u}\otimes\boldsymbol{v})_{ij} = u_i v_j, \quad (\boldsymbol{a}\otimes\boldsymbol{b})_{ijkl} = a_{ij}b_{kl}\,. \tag{A.2}$$

- Symbols $\mathbf{1}$ and $\boldsymbol{I}$ designate the second- and fourth–order symmetric identity tensors respectively:

$$\mathbf{1}_{ij} = \delta_{ij}, \quad \boldsymbol{I}_{ijkl} = \frac{1}{2}(\delta_{ik}\delta_{jl} + \delta_{il}\delta_{jk})\,, \tag{A.3}$$

  where $\delta_{ij} = 1$ if $i = j$, $\delta_{ij} = 0$ if $i \neq j$.

- The spherical and deviatoric operators are $\boldsymbol{I}^{\mathrm{vol}}$ and $\boldsymbol{I}^{\mathrm{dev}}$ respectively:

$$\boldsymbol{I}^{\mathrm{vol}} \equiv \frac{1}{3}\mathbf{1}\otimes\mathbf{1}, \quad \boldsymbol{I}^{\mathrm{dev}} = \boldsymbol{I} - \boldsymbol{I}^{\mathrm{vol}}\,, \tag{A.4}$$

so that for symmetric tensors $a_{ij} = a_{ji}$ we have:

$$\boldsymbol{I}^{\mathrm{vol}} : \boldsymbol{a} = \frac{1}{3}a_{mm}\mathbf{1}\,, \quad \boldsymbol{I}^{\mathrm{dev}} : \boldsymbol{a} = \boldsymbol{a} - \frac{1}{3}a_{mm}\mathbf{1} = \mathrm{dev}(\boldsymbol{a})\,. \tag{A.5}$$

Appendix B. Derivation of the closed-form expressions for the incremental–secant method

Appendix B.1. Incremental–secant operator $\boldsymbol{C}^S$

During MFH process, in order to identify κ and μ_s –standing for either κ^{r} and μ_s^{r} or κ^0 and μ_s^0– the elastic bulk and shear moduli of the virtual elastic material, the increments of the stress and strain tensors are decomposed into their hydrostatic and deviatoric parts:

$$\Delta\boldsymbol{\sigma} = \Delta\sigma^m\mathbf{1} + \Delta\boldsymbol{s} \quad \text{and} \quad \Delta\boldsymbol{\varepsilon} = \Delta\varepsilon^m\mathbf{1} + \Delta\boldsymbol{e}\,, \tag{B.1}$$

where $\Delta\sigma^m = \frac{1}{3}\mathrm{tr}(\Delta\boldsymbol{\sigma})$, $\Delta\boldsymbol{s} = \Delta\boldsymbol{\sigma} - \Delta\sigma^m\mathbf{1}$, $\Delta\varepsilon^m = \frac{1}{3}\mathrm{tr}(\Delta\boldsymbol{\varepsilon})$, and $\Delta\boldsymbol{e} = \Delta\boldsymbol{\varepsilon} - \Delta\varepsilon^m\mathbf{1}$. Note that $\Delta\boldsymbol{\sigma} = \boldsymbol{\sigma}$ when the zero–incremental–secant operator $\boldsymbol{C}^{\mathrm{S0}}$ is used in the MFH process.

Following the developments of Wu et al. (Submitted), the elastic bulk modulus $\kappa = \kappa^{\mathrm{el}}$ remains constant because of the incompressible nature of the plastic flow, and

$$3\mu_s = \frac{\Delta\sigma^{\mathrm{eq}}}{\Delta\varepsilon^{\mathrm{eq}}}\,, \tag{B.2}$$

with

$$\Delta\sigma^{\mathrm{eq}} = (\frac{3}{2}\Delta\boldsymbol{s} : \Delta\boldsymbol{s})^{1/2} \quad \text{and} \quad \Delta\varepsilon^{\mathrm{eq}} = (\frac{2}{3}\Delta\boldsymbol{e} : \Delta\boldsymbol{e})^{1/2}\,. \tag{B.3}$$

The derivative of the tensor –with $\boldsymbol{C}^{\mathrm{S}}$ standing for either $\boldsymbol{C}^{\mathrm{Sr}}$ or $\boldsymbol{C}^{\mathrm{S0}}$– is expressed as

$$\frac{\partial\boldsymbol{C}^{\mathrm{S}}}{\partial\boldsymbol{\varepsilon}} = 2\boldsymbol{I}^{\mathrm{dev}} \otimes \left[\frac{1}{6\mu_s\left(\Delta\varepsilon^{\mathrm{eq}}\right)^2}\Delta\boldsymbol{s} : \boldsymbol{C}^{\mathrm{alg}} - \frac{2}{3}\mu_s\frac{\Delta\boldsymbol{e}}{\left(\Delta\varepsilon^{\mathrm{eq}}\right)^2}\right]\,, \tag{B.4}$$

where the "consistent" operator $\boldsymbol{C}^{\mathrm{alg}}$ is the derivative of the stress increment with respect to the strain increment, which is obtained from the constitutive law of the material, see Appendix C.

Appendix B.2. Damaged incremental–secant operator $\boldsymbol{C}^{SD}$

In order to apply the MFH scheme we need to know $\frac{\partial \boldsymbol{C}^{\mathrm{SD}}}{\partial \boldsymbol{\varepsilon}}$ –with $\boldsymbol{C}^{\mathrm{SD}}$ standing for either $\boldsymbol{C}^{\mathrm{SDr}}$ or $\boldsymbol{C}^{\mathrm{SD0}}$. One has directly

$$\frac{\partial \boldsymbol{C}^{\mathrm{SD}}}{\partial \boldsymbol{\varepsilon}} \;=\; (1-D)\,\frac{\partial \boldsymbol{C}^{\mathrm{S}}}{\partial \boldsymbol{\varepsilon}} - \boldsymbol{C}^{\mathrm{S}} \otimes \frac{\partial D}{\partial \boldsymbol{\varepsilon}}\,, \tag{B.5}$$

where $\frac{\partial \boldsymbol{C}^{\mathrm{S}}}{\partial \boldsymbol{\varepsilon}}$ has the same expression as in Appendix B.1, and where $\frac{\partial D}{\partial \boldsymbol{\varepsilon}}$ is given in Appendix C.

As the non-local variable $\tilde{p}$ is used during the damage evaluation, we also have to determine

$$\frac{\partial \boldsymbol{C}^{\mathrm{SD}}}{\partial \tilde{p}} = -\frac{\partial D}{\partial \tilde{p}} \boldsymbol{C}^{\mathrm{S}}\,, \tag{B.6}$$

where $\frac{\partial D}{\partial \tilde{p}}$ is given in Appendix C.

Appendix C. Linearization of the Lemaitre–Chaboche ductile damage model in the non–local form

During a finite incremental process, the constitutive equations are discretized in time intervals $[t_n,\, t_{n+1}]$, and the constitutive equations are differentiated at t_{n+1}. Remembering that for the non–local formulation the damage depends on both $\boldsymbol{\varepsilon}$ and on $\tilde{p}$, this linearization reads

$$\delta\boldsymbol{\sigma}_{n+1} = \boldsymbol{C}^{\mathrm{algD}} : \delta\boldsymbol{\varepsilon}_{n+1} - \left(\hat{\boldsymbol{\sigma}}_{n+1} \otimes \frac{\partial D}{\partial \boldsymbol{\varepsilon}}\right) : \delta\boldsymbol{\varepsilon}_{n+1} - \hat{\boldsymbol{\sigma}}_{n+1}\frac{\partial D}{\partial \tilde{p}}\delta\tilde{p}_{n+1}\,, \tag{C.1}$$

where

$$\boldsymbol{C}^{\mathrm{algD}} = (1-D_{n+1})\boldsymbol{C}^{\mathrm{alg}}\,. \tag{C.2}$$

In these last expressions, $\boldsymbol{C}^{\mathrm{alg}} = \frac{\partial \hat{\boldsymbol{\sigma}}_{n+1}}{\partial \boldsymbol{\varepsilon}} = \frac{\partial \hat{\boldsymbol{\sigma}}_{n+1}}{\partial \Delta\boldsymbol{\varepsilon}^{\mathrm{r}}}$ is the derivative of the effective stress increment with respect to the strain increment[9], which ensures quadratic convergence, as shown by Simo and Taylor (1985).

This expression is now derived for the residual–incremental–secant approach presented in Section 3.2.1. In particular the effect of the assumption

[9] In this non–local formalism, we explicitly write the dependence of the stress in D and $\boldsymbol{\varepsilon}$ and linearize with respect to both terms. We use symbol $\boldsymbol{C}^{\mathrm{alg}}$ for the derivative of the effective stress increment with respect to the strain increment.

in the plastic flow direction is accounted for. From Eqs. (29) and (30) one has directly

$$\boldsymbol{C}^{\mathrm{alg}} = \boldsymbol{C}^{\mathrm{el}} - 2\mu^{\mathrm{el}}\boldsymbol{N} \otimes \frac{\partial \Delta p}{\partial \boldsymbol{\varepsilon}} - 2\mu^{\mathrm{el}}\Delta p \frac{\partial \boldsymbol{N}}{\partial \boldsymbol{\varepsilon}} \,. \tag{C.3}$$

On the one hand, using $\frac{\partial \boldsymbol{a}^{\mathrm{eq}}}{\partial \boldsymbol{a}} = \frac{3}{2}\frac{\boldsymbol{a}^{\mathrm{dev}}}{\boldsymbol{a}^{\mathrm{eq}}}$, the two Eqs. (33-34) of the system related to the yield surface evolution lead to

$$\frac{3}{2}\frac{(\hat{\boldsymbol{\sigma}}_{n+1} - \hat{\boldsymbol{\sigma}}_n^{\mathrm{res}})^{\mathrm{dev}}}{(\hat{\boldsymbol{\sigma}}_{n+1} - \hat{\boldsymbol{\sigma}}_n^{\mathrm{res}})^{\mathrm{eq}}} : \left[\frac{1}{3}\left(\frac{3}{2}\frac{(\hat{\boldsymbol{\sigma}}_{n+1})^{\mathrm{dev}}}{(\hat{\boldsymbol{\sigma}}_{n+1})^{\mathrm{eq}}}\right)^{-1}\frac{\partial R}{\partial p}\delta p\right] + 3\mu^{\mathrm{el}}\delta p = \frac{3}{2}\frac{\left(\hat{\boldsymbol{\sigma}}_{n+1}^{\mathrm{tr}} - \hat{\boldsymbol{\sigma}}_n^{\mathrm{res}}\right)^{\mathrm{dev}}}{\left(\hat{\boldsymbol{\sigma}}_{n+1}^{\mathrm{tr}} - \hat{\boldsymbol{\sigma}}_n^{\mathrm{res}}\right)^{\mathrm{eq}}} : \boldsymbol{C}^{\mathrm{el}} : \delta\boldsymbol{\varepsilon} \,, \tag{C.4}$$

which can be rewritten, using Eqs. (31) and (32) and calling $\boldsymbol{N}^0 = \frac{3}{2}\frac{(\hat{\boldsymbol{\sigma}}_{n+1})^{\mathrm{dev}}}{(\hat{\boldsymbol{\sigma}}_{n+1})^{\mathrm{eq}}}$ the normal to the yield surface, as

$$\frac{\partial p}{\partial \boldsymbol{\varepsilon}} = \frac{2\mu^{\mathrm{el}}}{h}\boldsymbol{N} \,, \tag{C.5}$$

with $h = \frac{1}{3}\boldsymbol{N} : (\boldsymbol{N}^0)^{-1}\frac{\partial R}{\partial p} + 3\mu^{\mathrm{el}}$. On the other hand, using $\frac{\partial \boldsymbol{a}^{\mathrm{dev}}}{\partial \boldsymbol{a}} = \boldsymbol{I}^{\mathrm{dev}}$, Eq. (32) yields

$$\frac{\partial \boldsymbol{N}}{\partial \boldsymbol{\varepsilon}} = \frac{3}{2}\frac{\boldsymbol{I}^{\mathrm{dev}} : \boldsymbol{C}^{\mathrm{el}}}{\left(\boldsymbol{C}^{\mathrm{el}} : \Delta\boldsymbol{\varepsilon}_{n+1}^{\mathrm{r}}\right)^{\mathrm{eq}}} - \frac{2\mu^{\mathrm{el}}\boldsymbol{N} \otimes \boldsymbol{N}}{\left(\boldsymbol{C}^{\mathrm{el}} : \Delta\boldsymbol{\varepsilon}_{n+1}^{\mathrm{r}}\right)^{\mathrm{eq}}} \,. \tag{C.6}$$

Finally, combining Eqs. (C.3), (C.5) and (32) leads to the final expression of the "consistent" operator

$$\boldsymbol{C}^{\mathrm{alg}} = \boldsymbol{C}^{\mathrm{el}} - \frac{\left(2\mu^{\mathrm{el}}\right)^2}{h}\boldsymbol{N} \otimes \boldsymbol{N} - \frac{\left(2\mu^{\mathrm{el}}\right)^2 \Delta p}{\left(\hat{\boldsymbol{\sigma}}_{n+1}^{\mathrm{tr}} - \hat{\boldsymbol{\sigma}}_n^{\mathrm{res}}\right)^{\mathrm{eq}}}\left(\frac{3}{2}\boldsymbol{I}^{\mathrm{dev}} - \boldsymbol{N} \otimes \boldsymbol{N}\right) \,. \tag{C.7}$$

For the zero–incremental–secant approach presented in Section 3.2.2 the same way of proceeding results in

$$\boldsymbol{C}^{\mathrm{alg}} = \boldsymbol{C}^{\mathrm{el}} - \frac{(2\mu^{\mathrm{el}})^2}{h_0}\boldsymbol{N} \otimes \boldsymbol{N} - \frac{(2\mu^{\mathrm{el}})^2 \Delta p}{\left(\hat{\boldsymbol{\sigma}}_{n+1}^{\mathrm{tr}}\right)^{\mathrm{eq}}}\left(\frac{3}{2}\boldsymbol{I}^{\mathrm{dev}} - \boldsymbol{N} \otimes \boldsymbol{N}\right) \,, \tag{C.8}$$

with $h_0 = 3\mu^{\mathrm{el}} + \frac{\mathrm{d}R}{\mathrm{d}p} > 0$ and $\boldsymbol{N} = \boldsymbol{N}^0$. In this case the direction of the normal corresponds strictly to the radial return mapping assumption, and the classical expression of $\boldsymbol{C}^{\mathrm{alg}}$ is recovered, e.g. (Doghri, 2000, chapter 12).

Moreover, it can be easily deduced from (21) that

$$\frac{\partial Y}{\partial \boldsymbol{\varepsilon}^{\mathrm{e}}} : \frac{\partial \boldsymbol{\varepsilon}^{\mathrm{e}}}{\partial \boldsymbol{\varepsilon}} : \delta\boldsymbol{\varepsilon} = \boldsymbol{\varepsilon}^{\mathrm{e}} : \boldsymbol{C}^{\mathrm{alg}} : \delta\boldsymbol{\varepsilon}\,, \tag{C.9}$$

leading to

$$\begin{aligned}
\delta D(\boldsymbol{\varepsilon}, \tilde{p}) &\approx \frac{\partial \Delta D}{\partial Y}\frac{\partial Y}{\partial \boldsymbol{\varepsilon}^{\mathrm{e}}} : \frac{\partial \boldsymbol{\varepsilon}^{\mathrm{e}}}{\partial \boldsymbol{\varepsilon}} : \delta\boldsymbol{\varepsilon} + \frac{\partial \Delta D}{\partial \tilde{p}}\delta\tilde{p} \\
&= s\Delta\tilde{p}\frac{(Y_{n+\alpha})^{s-1}}{S_0^s}\frac{\partial Y}{\partial \boldsymbol{\varepsilon}^{\mathrm{e}}} : \frac{\partial \boldsymbol{\varepsilon}^{\mathrm{e}}}{\partial \boldsymbol{\varepsilon}} : \delta\boldsymbol{\varepsilon} + (\frac{Y_{n+\alpha}}{S_0})^s\delta\tilde{p} \\
&= \alpha s\Delta\tilde{p}\frac{(Y_{n+\alpha})^{s-1}}{S_0^s}\boldsymbol{\varepsilon}^{\mathrm{e}} : \boldsymbol{C}^{\mathrm{alg}} : \delta\boldsymbol{\varepsilon} + (\frac{Y_{n+\alpha}}{S_0})^s\delta\tilde{p}\,.
\end{aligned} \tag{C.10}$$

Appendix D. Stress residual vector

The equation to be satisfied at the end of the MFH procedure is Eq. (17). Multiplying Eq. (15) by $\boldsymbol{B}^{\epsilon}\left(\boldsymbol{I}, \bar{\boldsymbol{C}}_0^{\mathrm{SD}}, \bar{\boldsymbol{C}}_{\mathrm{I}}^{\mathrm{S}}\right)$ and using (17) lead to

$$v_0\Delta\boldsymbol{\varepsilon}^{\mathrm{r}}_{\mathrm{I}n+1} + v_{\mathrm{I}}\boldsymbol{B}^{\epsilon}(\boldsymbol{I}, \bar{\boldsymbol{C}}_0^{\mathrm{SD}}, \bar{\boldsymbol{C}}_{\mathrm{I}}^{\mathrm{S}}) : \Delta\boldsymbol{\varepsilon}^{\mathrm{r}}_{\mathrm{I}n+1} = \boldsymbol{B}^{\epsilon}(\boldsymbol{I}, \bar{\boldsymbol{C}}_0^{\mathrm{SD}}, \bar{\boldsymbol{C}}_{\mathrm{I}}^{\mathrm{S}}) : \Delta\bar{\boldsymbol{\varepsilon}}^{\mathrm{r}}_{n+1}\,. \tag{D.1}$$

With the M-T assumption the strain concentration tensor follows from (4), and Eq. (D.1) reads

$$\Delta\boldsymbol{\varepsilon}^{\mathrm{r}}_{\mathrm{I}n+1} + v_0\boldsymbol{S} : \left[\left(\bar{\boldsymbol{C}}_0^{\mathrm{SD}}\right)^{-1} : \bar{\boldsymbol{C}}_{\mathrm{I}}^{\mathrm{S}} - \boldsymbol{I}\right] : \Delta\boldsymbol{\varepsilon}^{\mathrm{r}}_{\mathrm{I}n+1} = \Delta\bar{\boldsymbol{\varepsilon}}^{\mathrm{r}}_{n+1}\,, \tag{D.2}$$

or again $\boldsymbol{F} = 0$ with

$$\boldsymbol{F} = \bar{\boldsymbol{C}}_0^{\mathrm{SD}} : \left[\Delta\boldsymbol{\varepsilon}^{\mathrm{r}}_{\mathrm{I}n+1} - \frac{1}{v_0}\boldsymbol{S}^{-1} : \left(\Delta\boldsymbol{\varepsilon}^{\mathrm{r}}_{\mathrm{I}n+1} - \Delta\bar{\boldsymbol{\varepsilon}}^{\mathrm{r}}_{n+1}\right)\right] - \bar{\boldsymbol{C}}_{\mathrm{I}}^{\mathrm{S}} : \Delta\boldsymbol{\varepsilon}^{\mathrm{r}}_{\mathrm{I}n+1}\,. \tag{D.3}$$

In order to satisfy $\boldsymbol{F} = 0$, Eq. (D.3) is linearized as[10]

$$\mathrm{d}\boldsymbol{F} = \frac{\partial \boldsymbol{F}}{\partial \boldsymbol{\varepsilon}_{\mathrm{I}}} : \mathrm{d}\Delta\boldsymbol{\varepsilon}^{\mathrm{r}}_{\mathrm{I}} + \frac{\partial \boldsymbol{F}}{\partial \boldsymbol{\varepsilon}_0} : \mathrm{d}\Delta\boldsymbol{\varepsilon}^{\mathrm{r}}_0 + \frac{\partial \boldsymbol{F}}{\Delta\bar{\boldsymbol{\varepsilon}}} : \mathrm{d}\Delta\bar{\boldsymbol{\varepsilon}}^{\mathrm{r}} + \frac{\partial \boldsymbol{F}}{\partial \tilde{p}}\mathrm{d}\tilde{p}\,. \tag{D.4}$$

[10] Note that the derivative with respect to $\Delta\boldsymbol{\varepsilon}^{\mathrm{r}}_r$ has the same expression as the derivative with respect to $\boldsymbol{\varepsilon}_r$

When solving $\boldsymbol{F}=0$ at constant $\Delta\bar{\boldsymbol{\varepsilon}}^{\mathrm{r}}$ and constant $\tilde{p}$, as $v_0\Delta\boldsymbol{\varepsilon}_0^{\mathrm{r}}+v_{\mathrm{I}}\Delta\boldsymbol{\varepsilon}_{\mathrm{I}}^{\mathrm{r}}$ is also constant, the iteration process relies on $\mathrm{d}\boldsymbol{F}=\boldsymbol{J}:\mathrm{d}\boldsymbol{\varepsilon}_{\mathrm{I}}$ with

$$\begin{aligned}
\boldsymbol{J} &= \frac{\partial \boldsymbol{F}}{\partial \boldsymbol{\varepsilon}_{\mathrm{I}}}+\frac{\partial \boldsymbol{F}}{\partial \boldsymbol{\varepsilon}_0}:\frac{\partial \boldsymbol{\varepsilon}_0}{\partial \boldsymbol{\varepsilon}_{\mathrm{I}}} \\
&= \bar{\boldsymbol{C}}_{0\ n+1}^{\mathrm{SD}}:\left[\boldsymbol{I}-\boldsymbol{S}^{-1}\right]-\bar{\boldsymbol{C}}_{\mathrm{I}\,n+1}^{\mathrm{S}}-\frac{\partial \bar{\boldsymbol{C}}_{\mathrm{I}\,n+1}^{\mathrm{S}}}{\partial \boldsymbol{\varepsilon}_{\mathrm{I}}}:\Delta\boldsymbol{\varepsilon}_{\mathrm{I}\,n+1}^{\mathrm{r}}- \\
&\quad \frac{v_{\mathrm{I}}}{v_0}\left(\frac{\partial \bar{\boldsymbol{C}}_{0\ n+1}^{\mathrm{SD}}}{\partial \boldsymbol{\varepsilon}_0}+\frac{\partial \bar{\boldsymbol{C}}_{0\ n+1}^{\mathrm{SD}}}{\partial D}\frac{\partial D}{\partial \boldsymbol{\varepsilon}_0}\right): \\
&\quad \left[\Delta\boldsymbol{\varepsilon}_{\mathrm{I}\,n+1}^{\mathrm{r}}-\boldsymbol{S}^{-1}:\frac{\left(\Delta\boldsymbol{\varepsilon}_{\mathrm{I}\,n+1}^{\mathrm{r}}-\Delta\bar{\boldsymbol{\varepsilon}}_{n+1}^{\mathrm{r}}\right)}{v_0}\right]- \\
&\quad \frac{v_{\mathrm{I}}}{v_0^2}\bar{\boldsymbol{C}}_{0\ n+1}^{\mathrm{SD}}\otimes\left(\Delta\boldsymbol{\varepsilon}_{\mathrm{I}\,n+1}^{\mathrm{r}}-\Delta\bar{\boldsymbol{\varepsilon}}_{n+1}^{\mathrm{r}}\right)::\\
&\quad \left(\boldsymbol{S}^{-1}\otimes\boldsymbol{S}^{-1}\right)::\left(\frac{\partial \boldsymbol{S}}{\partial \boldsymbol{\varepsilon}_0}+\frac{\partial \boldsymbol{S}}{\partial D}\frac{\partial D}{\partial \boldsymbol{\varepsilon}_0}\right)-\frac{v_{\mathrm{I}}}{v_0}\bar{\boldsymbol{C}}_{0\ n+1}^{\mathrm{SD}}:\boldsymbol{S}^{-1}\,, \qquad \text{(D.5)}
\end{aligned}$$

where $\frac{\partial \bar{\boldsymbol{C}}_{\mathrm{I}}^{\mathrm{S}}}{\partial \boldsymbol{\varepsilon}_{\mathrm{I}}}$ results from (B.4), and where $\frac{d\bar{\boldsymbol{C}}_0^{\mathrm{SD}}}{d\boldsymbol{\varepsilon}_0}=\frac{\partial \bar{\boldsymbol{C}}_{0\ n+1}^{\mathrm{SD}}}{\partial \boldsymbol{\varepsilon}_0}+\frac{\partial \bar{\boldsymbol{C}}_{0\ n+1}^{\mathrm{SD}}}{\partial D}\frac{\partial D}{\partial \boldsymbol{\varepsilon}_0}$ results from (B.5). The derivative of the Eshelby tensor $\frac{\partial \boldsymbol{S}}{\partial \boldsymbol{\varepsilon}_0}=\left(\frac{\partial \boldsymbol{S}}{\partial \boldsymbol{\varepsilon}_0}+\frac{\partial \boldsymbol{S}}{\partial D}\frac{\partial D}{\partial \boldsymbol{\varepsilon}_0}\right)$ is reported in Appendix F.

Once $\boldsymbol{F}=0$ is satisfied, the effect on the strain increment in each phase of a variation $\mathrm{d}\Delta\bar{\boldsymbol{\varepsilon}}^{\mathrm{r}}$ at constant $\Delta\tilde{p}$ can directly be obtained by constraining $\mathrm{d}\boldsymbol{F}=0$, and Eq. (D.4) leads to

$$0 = \frac{\partial \boldsymbol{F}}{\partial \boldsymbol{\varepsilon}_{\mathrm{I}}}:\mathrm{d}\Delta\boldsymbol{\varepsilon}_{\mathrm{I}}^{\mathrm{r}}+\frac{\partial \boldsymbol{F}}{\partial \boldsymbol{\varepsilon}_0}:\mathrm{d}\Delta\boldsymbol{\varepsilon}_0^{\mathrm{r}}+\frac{\partial \boldsymbol{F}}{\partial \bar{\boldsymbol{\varepsilon}}}:\mathrm{d}\Delta\bar{\boldsymbol{\varepsilon}}^{\mathrm{r}}\,, \qquad \text{(D.6)}$$

or again

$$\frac{\partial \boldsymbol{\varepsilon}_{\mathrm{I}}}{\partial \bar{\boldsymbol{\varepsilon}}} = -\boldsymbol{J}^{-1}:\frac{\partial \boldsymbol{F}}{\partial \bar{\boldsymbol{\varepsilon}}}\,. \qquad \text{(D.7)}$$

As under these circumstances $\mathrm{d}\bar{\boldsymbol{\varepsilon}}^{\mathrm{r}}=v_0\mathrm{d}\boldsymbol{\varepsilon}_0^{\mathrm{r}}+v_{\mathrm{I}}\mathrm{d}\boldsymbol{\varepsilon}_{\mathrm{I}}^{\mathrm{r}}$, this last equation is completed by

$$\frac{\partial \boldsymbol{\varepsilon}_0}{\partial \bar{\boldsymbol{\varepsilon}}} = \frac{1}{v_0}(\boldsymbol{I}-v_1\frac{\partial \boldsymbol{\varepsilon}_{\mathrm{I}}}{\partial \bar{\boldsymbol{\varepsilon}}})\,. \qquad \text{(D.8)}$$

The same relations can be obtained for a linearization with respect to $\tilde{p}$ at constant $\Delta\bar{\boldsymbol{\varepsilon}}^{\mathrm{r}}$.

Appendix E. "Consistent" linearization of the homogenized stress

The "consistent" linearization of the homogenized stress can be rewritten using Eqs. (57) and (C.1) for the homogenized material, leading to

$$\begin{aligned}
\delta\bar{\boldsymbol{\sigma}} &= v_{\mathrm{I}}\delta\boldsymbol{\sigma}_{\mathrm{I}} + v_0\delta\boldsymbol{\sigma}_0 \\
&= v_{\mathrm{I}}\boldsymbol{C}_{\mathrm{I}}^{\mathrm{alg}} : \delta\boldsymbol{\varepsilon}_{\mathrm{I}} + v_0\left(\boldsymbol{C}_0^{\mathrm{algD}} - \hat{\boldsymbol{\sigma}}_0 \otimes \frac{\partial D}{\partial \boldsymbol{\varepsilon}_0}\right) : \delta\boldsymbol{\varepsilon}_0 - v_0\hat{\boldsymbol{\sigma}}_0\frac{\partial D}{\partial \tilde{p}}\delta\tilde{p} \\
&= v_{\mathrm{I}}\boldsymbol{C}_{\mathrm{I}}^{\mathrm{alg}} : \left(\frac{\partial \boldsymbol{\varepsilon}_{\mathrm{I}}}{\partial \bar{\boldsymbol{\varepsilon}}} : \delta\bar{\boldsymbol{\varepsilon}} + \frac{\partial \boldsymbol{\varepsilon}_{\mathrm{I}}}{\partial \tilde{p}}\delta\tilde{p}\right) + v_0\left(\boldsymbol{C}_0^{\mathrm{algD}} - \hat{\boldsymbol{\sigma}}_0 \otimes \frac{\partial D}{\partial \boldsymbol{\varepsilon}_0}\right) : \\
&\quad \left(\frac{\partial \boldsymbol{\varepsilon}_0}{\partial \bar{\boldsymbol{\varepsilon}}} : \delta\bar{\boldsymbol{\varepsilon}} + \frac{\partial \boldsymbol{\varepsilon}_0}{\partial \tilde{p}}\delta\tilde{p}\right) - v_0\hat{\boldsymbol{\sigma}}_0\frac{\partial D}{\partial \tilde{p}}\delta\tilde{p}\,, \qquad \text{(E.1)}
\end{aligned}$$

with, see Appendix D,

$$\frac{\partial \boldsymbol{\varepsilon}_{\mathrm{I}}}{\partial \bar{\boldsymbol{\varepsilon}}} = -\boldsymbol{J}^{-1} : \frac{\partial \boldsymbol{F}}{\partial \bar{\boldsymbol{\varepsilon}}} \quad , \quad \frac{\partial \boldsymbol{\varepsilon}_0}{\partial \bar{\boldsymbol{\varepsilon}}} = \frac{1}{v_0}(\boldsymbol{I} - v_1\frac{\partial \boldsymbol{\varepsilon}_{\mathrm{I}}}{\partial \bar{\boldsymbol{\varepsilon}}})\,, \qquad \text{(E.2)}$$

$$\frac{\partial \boldsymbol{\varepsilon}_{\mathrm{I}}}{\partial \tilde{p}} = -\boldsymbol{J}^{-1} : \frac{\partial \boldsymbol{F}}{\partial \tilde{p}} \quad , \text{ and } \quad \frac{\partial \boldsymbol{\varepsilon}_0}{\partial \tilde{p}} = -\frac{v_{\mathrm{I}}}{v_0}\frac{\partial \boldsymbol{\varepsilon}_{\mathrm{I}}}{\partial \tilde{p}}\,. \qquad \text{(E.3)}$$

Thus, the consistent tangent operators read

$$\bar{\boldsymbol{C}}_{n+1}^{\mathrm{alg}} = v_{\mathrm{I}}\boldsymbol{C}_{\mathrm{I}}^{\mathrm{alg}} : \frac{\partial \boldsymbol{\varepsilon}_{\mathrm{I}}}{\partial \bar{\boldsymbol{\varepsilon}}} + v_0\left(\boldsymbol{C}_0^{\mathrm{algD}} - \hat{\boldsymbol{\sigma}}_0 \otimes \frac{\partial D}{\partial \boldsymbol{\varepsilon}_0}\right) : \frac{\partial \boldsymbol{\varepsilon}_0}{\partial \bar{\boldsymbol{\varepsilon}}}\,, \qquad \text{(E.4)}$$

$$\begin{aligned}
\boldsymbol{C}_{\tilde{p}} &= v_{\mathrm{I}}\boldsymbol{C}_{\mathrm{I}}^{\mathrm{alg}} : \frac{\partial \boldsymbol{\varepsilon}_{\mathrm{I}}}{\partial \tilde{p}}\delta\tilde{p} + \\
&\quad v_0\left(\boldsymbol{C}_0^{\mathrm{algD}} - \hat{\boldsymbol{\sigma}}_0 \otimes \frac{\partial D}{\partial \boldsymbol{\varepsilon}_0}\right) : \frac{\partial \boldsymbol{\varepsilon}_0}{\partial \tilde{p}} - v_0\hat{\boldsymbol{\sigma}}_0\frac{\partial D}{\partial \tilde{p}}\,. \qquad \text{(E.5)}
\end{aligned}$$

Appendix F. Eshelby Tensor and its derivative

The derivative of the Eshelby tensor can be written as

$$\frac{\partial \boldsymbol{S}}{\partial \Delta\boldsymbol{\varepsilon}^{\mathrm{r}}} = \frac{\partial \boldsymbol{S}}{\partial \nu} \otimes \left(\frac{\partial \nu}{\partial \kappa}\frac{\partial \kappa}{\partial \Delta\boldsymbol{\varepsilon}^{\mathrm{r}}} + \frac{\partial \nu}{\partial \mu_s}\frac{\partial \mu_s}{\partial \Delta\boldsymbol{\varepsilon}^{\mathrm{r}}}\right). \qquad \text{(F.1)}$$

If damage is not considered, we have

$$\frac{\partial \kappa}{\partial \Delta\boldsymbol{\varepsilon}^{\mathrm{r}}} = 0\,, \qquad \text{(F.2)}$$

therefore,

$$\frac{\partial \boldsymbol{S}}{\partial \Delta \boldsymbol{\varepsilon}^{\mathrm{r}}} = \frac{\partial \boldsymbol{S}}{\partial \nu} \otimes \frac{\partial \nu}{\partial \mu_s} \frac{\partial \mu_s}{\partial \Delta \boldsymbol{\varepsilon}^{\mathrm{r}}} \,. \tag{F.3}$$

When damage is considered, the secant moduli with damage need to be used (see Eqs. (44-49)) to compute the Eshelby tensor, and its derivative reads

$$\begin{aligned} \frac{\partial \boldsymbol{S}}{\partial \Delta \boldsymbol{\varepsilon}^{\mathrm{r}}} &= \frac{\partial \boldsymbol{S}}{\partial \nu} \otimes \left(\frac{\partial \nu}{\partial \kappa^D} \frac{\partial \kappa^D}{\partial \Delta \boldsymbol{\varepsilon}^{\mathrm{r}}} + \frac{\partial \nu}{\partial \mu_s^D} \frac{\partial \mu_s^D}{\partial \Delta \boldsymbol{\varepsilon}^{\mathrm{r}}} \right) \\ &= \frac{\partial \boldsymbol{S}}{\partial \nu} \otimes \left[\frac{\partial \nu}{\partial \kappa^D} \left(\frac{\partial \kappa^D}{\partial \Delta \boldsymbol{\varepsilon}^{\mathrm{r}}} + \frac{\partial \kappa^D}{\partial D} \frac{\partial D}{\partial \Delta \boldsymbol{\varepsilon}^{\mathrm{r}}} \right) + \frac{\partial \nu}{\partial \mu_s^D} \left(\frac{\partial \mu_s^D}{\partial \Delta \boldsymbol{\varepsilon}^{\mathrm{r}}} + \frac{\partial \mu_s^D}{\partial D} \frac{\partial D}{\partial \Delta \boldsymbol{\varepsilon}^{\mathrm{r}}} \right) \right] . \end{aligned} \tag{F.4}$$

Acknowledgment

The research has been funded by the Walloon Region under the agreement SIMUCOMP n^o 1017232 (CT-EUC 2010-10-12) in the context of the ERA-NET +, Matera + framework.

References

Aboudi, J., Pindera, M.J., Arnold, S., 2003. Higher-order theory for periodic multiphase materials with inelastic phases. Int. J. Plasticity 19, 805 – 847.

Aifantis, E., 1992. On the role of gradients in the localization of deformation and fracture. Int. J. Eng. Sci. 30, 1279 – 1299.

Bažant, Z.P., Belytchko, T.B., Chang, T.P., 1984. Continuum theory for strain-softening. J. Eng. Mech.–ASCE 110, 1666–1692.

Benveniste, Y., 1987. A new approach to the application of Mori-Tanaka's theory in composite materials. Mech. Mater. 6, 147 – 157.

Berveiller, M., Zaoui, A., 1978. An extension of the self-consistent scheme to plastically-flowing polycrystals. J. Mech. Phys. Solids 26, 325 – 344.

Brassart, L., Stainier, L., Doghri, I., Delannay, L., 2011. A variational formulation for the incremental homogenization of elasto-plastic composites. J. Mech. Phys. Solids 59, 2455 – 2475.

Brassart, L., Stainier, L., Doghri, I., Delannay, L., 2012. Homogenization of elasto-(visco) plastic composites based on an incremental variational principle. Int. J. Plasticity 36, 86 – 112.

Byström, J., 2009. Optimal design of a long and slender compressive strut. Int. J. Multiphysics 3, 235–257.

Carrere, N., Valle, R., Bretheau, T., Chaboche, J.L., 2004. Multiscale analysis of the transverse properties of ti-based matrix composites reinforced by sic fibres: from the grain scale to the macroscopic scale. Int. J. Plasticity 20, 783 – 810.

Chaboche, J., Kanouté, P., Roos, A., 2005. On the capabilities of mean-field approaches for the description of plasticity in metal matrix composites. Int. J. Plasticity 21, 1409 – 1434.

Christman, T., Needleman, A., Nutt, S., Suresh, S., 1989. On microstructural evolution and micromechanical modelling of deformation of a whisker-reinforced metal-matrix composite. Mater. Sci. Eng.: A 107, 49 – 61. Proceedings of the Symposium on Interfacial Phenomena in Composites: Processing Characterization and Mechanical Properties.

Coenen, E., Kouznetsova, V., Geers, M., 2011a. Enabling microstructure-based damage and localization analyses and upscaling. Model. Simul. Mater. Sci. Eng. 19, 074008.

Coenen, E., Kouznetsova, V., Geers, M., 2011b. Novel boundary conditions for strain localization analyses in microstructural volume elements. Int. J. Numer. Meth. Eng. .

Corbin, S., Wilkinson, D., 1994. Influence of matrix strength and damage accumulation on the mechanical response of a particulate metal matrix composite. Acta Metall. et Mater. 42, 1329 – 1335.

Dascalu, C., 2009. A two-scale damage model with material length. CR Mécanique 337, 645 – 652.

De Borst, R., 1991. Simulation of strain localization: a reappraisal of the Cosserat continuum. Eng. Comput. 8, 317 – 332.

De Borst, R., Sluys, L., Mühlhaus, H.B., Pamin, J., 1993. Fundamental issues in finite element analyses of localization of deformation. Eng. Comput. 10, 99 – 121.

Doghri, I., 1995. Numerical implementation and analysis of a class of metal plasticity models coupled with ductile damage. Int. J. Numer. Meth. Eng. 38, 3403–3431.

Doghri, I., 2000. Mechanics of Deformable Solids- Linear, Nonlinear, Analytical and Computational Aspects. Springer-Verlag, Berlin.

Doghri, I., Adam, L., Bilger, N., 2010. Mean-field homogenization of elasto-viscoplastic composites based on a general incrementally affine linearization method. Int. J. Plasticity 26, 219 – 238.

Doghri, I., Brassart, L., Adam, L., Gérard, J.S., 2011. A second-moment incremental formulation for the mean-field homogenization of elasto-plastic composites. Int. J. Plasticity 27, 352 – 371.

Doghri, I., Ouaar, A., 2003. Homogenization of two-phase elasto-plastic composite materials and structures: Study of tangent operators, cyclic plasticity and numerical algorithms. Int. J. Solids Struct. 40, 1681 – 1712.

Doghri, I., Tinel, L., 2005. Micromechanical modeling and computation of elasto-plastic materials reinforced with distributed-orientation fibers. Int. J. Plasticity 21, 1919 – 1940.

Engelen, R.A.B, M., Baaijens, F., 2003. Nonlocal implicit gradient-enhanced elasto-plasticity for the modelling of softening behaviour. Int. J. Plasticity 19, 403 – 433.

Eshelby, J.D., 1957. The determination of the elastic field of an ellipsoidal inclusion, and related problems. Proceedings of the Royal Society of London. Series A, Mathematical and Physical Sciences 241, pp. 376–396.

Geers, M., 1997. Experimental Analysis and Computational Modelling of Damage and Fracture. Ph.D. thesis. University of Technology, Eindhoven (Netherlands).

Geers, M., de Borst, R., Brekelmans, W., Peerlings, R., 1999. Validation and internal length scale determination for a gradient damage model: application to short glass-fibre-reinforced polypropylene. Int. J. Solids Struct. 36, 2557 – 2583.

Geers, M., Kouznetsova, V., Brekelmans, A., 2010. Multi-scale computational homogenization: Trends and challenges. J. Comput. Appl. Math. 234, 2175 – 2182.

Geers, M.G.D., de Borst, R., Brekelmans, W.A.M., Peerlings, R.H.J., 1998. Strain-based transient-gradient damage model for failure analyses. Comput. Methods Appl. Mech. Eng. 160, 133–153.

Hill, R., 1965a. Continuum micro-mechanics of elastoplastic polycrystals. J. Mech. Phys. Solids 13, 89 – 101.

Hill, R., 1965b. A self-consistent mechanics of composite materials. J. Mech. Phys. Solids 13, 213 – 222.

Ji, B., Wang, T., 2003. Plastic constitutive behavior of short-fiber/particle reinforced composites. Int. J. Plasticity 19, 565 – 581.

Kanouté, P., Boso, D., Chaboche, J., Schrefler, B., 2009. Multiscale methods for composites: A review. Arch. Comput. Methods Eng. 16, 31–75. 10.1007/s11831-008-9028-8.

Knockaert, R., Doghri, I., 1999. Nonlocal constitutive models with gradients of internal variables derived from a micro/macro homogenization procedure. Comput. Methods Appl. Mech. Eng. 174, 121 – 136.

Kouznetsova, V., Geers, M., Brekelmans, W., 2004. Multi-scale second-order computational homogenization of multi-phase materials: a nested finite element solution strategy. Comput. Methods Appl. Mech. Eng. 193, 5525 – 5550. Adv. Comput. Plasticity.

Kouznetsova, V., Geers, M.G.D., Brekelmans, W.A.M., 2002. Multi-scale constitutive modelling of heterogeneous materials with a gradient-enhanced computational homogenization scheme. Int. J. Numer. Meth. Eng. 54, 1235–1260.

Kröner, E., 1958. Berechnung der elastischen konstanten des vielkristalls aus den konstanten des einkristalls. Z Phys. A–Hadron Nucl. 151, 504–518. 10.1007/BF01337948.

Lahellec, N., Ponte Castañeda, P., Suquet, P., 2011. Variational estimates for the effective response and field statistics in thermoelastic composites with intra-phase property fluctuations. Proceedings of the Royal Society A: Mathematical, Physical and Engineering Science 467, 2224–2246.

Lahellec, N., Suquet, P., 2007a. On the effective behavior of nonlinear inelastic composites: I. incremental variational principles. J. Mech. Phys. Solids 55, 1932 – 1963.

Lahellec, N., Suquet, P., 2007b. On the effective behavior of nonlinear inelastic composites: II. a second-order procedure. J. Mech. Phys. Solids 55, 1964 – 1992.

Lahellec, N., Suquet, P., 2013. Effective response and field statistics in elasto-plastic and elasto-viscoplastic composites under radial and non-radial loadings. Int. J. Plasticity .

Lemaitre, J., 1985. Coupled elasto-plasticity and damage constitutive equations. Comput. Methods Appl. Mech. Eng. 51, 31 – 49.

Lemaitre, J., Chaboche, J.L., 1991. Mécanique des Matériaux solides. Dunod.

Lemaitre, J., Desmorat, R., 2005. Engineering damage mechanics: ductile, creep, fatigue and brittle failures. Springer-Verlag, Berlin.

Lissenden, C., Arnold, S., 1997. Theoretical and experimental considerations in representing macroscale flow/damage surfaces for metal matrix composites. Int. J. Plasticity 13, 327 – 358.

Liu, X., Hu, G., 2005. A continuum micromechanical theory of overall plasticity for particulate composites including particle size effect. Int. J. Plasticity 21, 777 – 799.

LLorca, J., González, C., Molina-Aldareguía, J.M., Segurado, J., Seltzer, R., Sket, F., Rodríguez, M., Sádaba, S., Muñoz, R., Canal, L.P., 2011. Multiscale modeling of composite materials: a roadmap towards virtual testing. Adv. Mater. 23, 5130–5147.

Massart, T., Peerlings, R., Geers, M., 2005. A dissipation-based control method for the multi-scale modelling of quasi-brittle materials. CR Mécanique 333, 521527.

Massart, T., Peerlings, R., Geers, M., 2007. An enhanced multi-scale approach for masonry wall computations. Int. J. Numer. Meth. Eng. 69, 1022–1059.

Masson, R., Bornert, M., Suquet, P., Zaoui, A., 2000. An affine formulation for the prediction of the effective properties of nonlinear composites and polycrystals. J. Mech. Phys. Solids 48, 1203 – 1227.

Mercier, S., Molinari, A., 2009. Homogenization of elasticviscoplastic heterogeneous materials: Self-consistent and Mori-Tanaka schemes. Int. J. Plasticity 25, 1024 – 1048.

Molinari, A., Canova, G., Ahzi, S., 1987. A self consistent approach of the large deformation polycrystal viscoplasticity. Acta Metall. 35, 2983–2994.

Molinari, A., El Houdaigui, F., Tóth, L., 2004. Validation of the tangent formulation for the solution of the non-linear eshelby inclusion problem. Int. J. Plasticity 20, 291 – 307.

Mori, T., Tanaka, K., 1973. Average stress in matrix and average elastic energy of materials with misfitting inclusions. Acta Metall. 21, 571–574. Cited By (since 1996) 1814.

Moulinec, H., Suquet, P., 2003. Intraphase strain heterogeneity in nonlinear composites: a computational approach. Eur. J. of Mech. - A/Solids 22, 751 – 770.

Peerlings, R., de Borst, R., Brekelmans, W., Ayyapureddi, S., 1996. Gradient-enhanced damage for quasi-brittle materials. Int. J. Numer. Meth. Eng. 39, 3391–3403.

Peerlings, R., de Borst, R., Brekelmans, W., Geers, M., 1998. Gradient-enhanced damage modelling of concrete fracture. Mech. Cohes.-Frict. Mater. 3, 323–342.

Peerlings, R., Geers, M., de Borst, R., Brekelmans, W., 2001. A critical comparison of nonlocal and gradient-enhanced softening continua. Int. J. Solids Struct. 38, 7723–7746.

Pettermann, H.E., Plankensteiner, A.F., Böhm, H.J., Rammerstorfer, F.G., 1999. A thermo-elasto-plastic constitutive law for inhomogeneous materials based on an incremental Mori-Tanaka approach. Comput. Struct. 71, 197 – 214.

Pierard, O., Doghri, I., 2006a. An enhanced affine formulation and the corresponding numerical algorithms for the mean-field homogenization of elasto-viscoplastic composites. Int. J. Plasticity 22, 131 – 157.

Pierard, O., Doghri, I., 2006b. Study of various estimates of the macroscopic tangent operator in the incremental homogenization of elastoplastic composites. Int. J. Multiscale Comput. Eng. 4, 521–543.

Pierard, O., LLorca, J., Segurado, J., Doghri, I., 2007. Micromechanics of particle-reinforced elasto-viscoplastic composites: Finite element simulations versus affine homogenization. Int. J. Plasticity 23, 1041 – 1060.

Ponte Castañeda, P., 1991. The effective mechanical properties of nonlinear isotropic composites. J. Mech. Phys. Solids 39, 45–71.

Ponte Castañeda, P., 1992. A new variational principle and its application to nonlinear heterogeneous systems. SIAM Journal on Applied Mathematics 52, 1321–1341.

Ponte Castañeda, P., 1996. Exact second-order estimates for the effective mechanical properties of nonlinear composite materials. J. Mech. Phys. Solids 44, 827 – 862.

Ponte Castañeda, P., 2002a. Second-order homogenization estimates for nonlinear composites incorporating field fluctuations: I - theory. J. Mech. Phys. Solids 50, 737 – 757.

Ponte Castañeda, P., 2002b. Second-order homogenization estimates for nonlinear composites incorporating field fluctuations: II - applications. J. Mech. Phys. Solids 50, 759 – 782.

Segurado, J., Llorca, J., González, C., 2002. On the accuracy of mean-field approaches to simulate the plastic deformation of composites. Scripta Mater. 46, 525 – 529.

Simo, J.C., Taylor, R.L., 1985. Consistent tangent operators for rate-independent elastoplasticity. Comput. Methods Appl. Mech. Eng. 48, 101 – 118.

Suquet, P., 1995. Overall properties of nonlinear composites: A modified secant moduli theory and its link with ponte castañeda's nonlinear variational procedure. CR Acad. Sci. 320, 563–571.

Svedberg, T., Runesson, K., 1997. A thermodynamically consistent theory of gradient-regularized plasticity coupled to damage. Int. J. Plasticity 13, 669 – 696.

Talbot, D., Willis, J., 1992. Some simple explicit bounds for the overall behaviour of nonlinear composites. Int. J. Solids Struct. 29, 1981 – 1987.

Talbot, D.R.S., Willis, J.R., 1985. Variational principles for inhomogeneous non-linear media. IMA J. Appl. Math. 35, 39–54.

Talbot, D.R.S., Willis, J.R., 1987. Bounds and self-consistent estimates for the overall properties of nonlinear composites. IMA J. Appl. Math. 39, 215–240.

Wieckowski, Z., 2000. Dual finite element methods in homogenization for elasticplastic fibrous composite material. Int. J. Plasticity 16, 199 – 221.

Wu, L., Noels, L., Adam, L., Doghri, I., 2012. Multiscale mean-field homogenization method for fiber-reinforced composites with gradient-enhanced damage model. Comput. Methods Appl. Mech. Eng. 233-236, 164–179.

Wu, L., Noels, L., Adam, L., Doghri, I., 2013. Non-local damage-enhanced mfh for multiscale simulations of composites, in: Composite Materials and Joining Technologies for Composites, Volume 7. Springer. chapter 13.

Wu, L., Noels, L., Adam, L., Doghri, I., Submitted. A combined incremental–secant mean–field homogenization scheme with per–phase residual strains for elasto–plastic composites. Int. J. Plasticity -, –.

Zaoui, A., Masson, R., 2002. Modelling stress-dependent transformation strains of heterogeneous materials, in: Bahei-El-Din, Y.A., Dvorak, G.J., Gladwell, G.M.L. (Eds.), IUTAM Symposium on Transformation Problems in Composite and Active Materials. Springer Netherlands. volume 60 of *Solid Mechanics and Its Applications*, pp. 3–15.

Zbib, H.M., Aifantis, E.C., 1989. A gradient-dependent flow theory of plasticity: Application to metal and soil instabilities. Appl. Mech. Rev.-T. ASME 42, S295–S304.